

University of Alberta

Optimal Solvent and Well Geometry for Production of Heavy Oil by Cyclic Solvent Injection

by

Jin Xiu Qi



A thesis submitted to the Faculty of Graduate Studies and Research in partial fulfillment of
the
requirements for the degree of Master of Science

in

Petroleum Engineering

Department of Civil & Environmental Engineering

Edmonton, Alberta

Fall 2005



Library and
Archives Canada

Bibliothèque et
Archives Canada

Published Heritage
Branch

Direction du
Patrimoine de l'édition

395 Wellington Street
Ottawa ON K1A 0N4
Canada

395, rue Wellington
Ottawa ON K1A 0N4
Canada

Your file *Votre référence*
ISBN: 978-0-494-22128-0
Our file *Notre référence*
ISBN: 978-0-494-22128-0

NOTICE:

The author has granted a non-exclusive license allowing Library and Archives Canada to reproduce, publish, archive, preserve, conserve, communicate to the public by telecommunication or on the Internet, loan, distribute and sell theses worldwide, for commercial or non-commercial purposes, in microform, paper, electronic and/or any other formats.

The author retains copyright ownership and moral rights in this thesis. Neither the thesis nor substantial extracts from it may be printed or otherwise reproduced without the author's permission.

AVIS:

L'auteur a accordé une licence non exclusive permettant à la Bibliothèque et Archives Canada de reproduire, publier, archiver, sauvegarder, conserver, transmettre au public par télécommunication ou par l'Internet, prêter, distribuer et vendre des thèses partout dans le monde, à des fins commerciales ou autres, sur support microforme, papier, électronique et/ou autres formats.

L'auteur conserve la propriété du droit d'auteur et des droits moraux qui protègent cette thèse. Ni la thèse ni des extraits substantiels de celle-ci ne doivent être imprimés ou autrement reproduits sans son autorisation.

In compliance with the Canadian Privacy Act some supporting forms may have been removed from this thesis.

Conformément à la loi canadienne sur la protection de la vie privée, quelques formulaires secondaires ont été enlevés de cette thèse.

While these forms may be included in the document page count, their removal does not represent any loss of content from the thesis.

Bien que ces formulaires aient inclus dans la pagination, il n'y aura aucun contenu manquant.


Canada

ABSTRACT

The Vapor Extraction (VAPEX) process has been proposed as an alternative to steam-based heavy oil recovery methods. In this process, a vaporized solvent is injected into a horizontal well and the diluted heavy oil is produced by gravity drainage from a horizontal producer situated below.

The dilution effect of the solvent is by diffusion into the oil. This is a rather slow process. The cyclic solvent soaking effect is examined through a compositional simulator, motivated by promoting a faster mass transfer mechanism.

The most effective solvent mixture is first determined through an Equation of State simulation and verified via a compositional simulator. The optimal soaking time for a certain injection rate is then investigated in order to optimize cyclic injection design.

Sensitivity analysis of well geometry on oil recovery is performed. As a result, the proper positioning of the injectors and producers is determined for achieving the highest cumulative production.

ACKNOWLEDGEMENTS

My foremost thank goes to my thesis advisor Dr. Marcel Polikar, I thank him for his support and encouragement that carried me through difficult times, and also for his suggestions and valuable feedback that greatly contributed to my dissertation.

I would gratefully thank the rest of my committee members, Dr. Luciane Cunha, who advised me on various aspects of my research at the early stages, and Dr. Carolina Diaz Goano, both for their valuable feedback which helped me to improve my dissertation in many ways.

In addition, I would like to acknowledge the financial support from the Natural Sciences and Engineering Research Council (NSERC) of Canada.

I would also like to take this opportunity to thank Ted Frauenfeld of ARC, Andrei Zaostrovski and Bruce Kohse of CMG for their priceless advice; Jiasen Tan of Schlumberger for his valuable help with the PVT data; and Tarek Hamida of the University of Alberta for his strong support in many difficult times.

Finally, I wish to sincerely thank my parents and my sister and brother for always being there when I need them.

TABLE OF CONTENTS

CHAPTER 1	1
INTRODUCTION	1
CHAPTER 2	3
LITERATURE REVIEW	3
2.1 VAPOR EXTRACTION (VAPEX).....	3
2.1.1 <i>What is VAPEX?</i>	3
2.1.2 <i>Why VAPEX?</i>	4
2.1.3 <i>Difficulties with VAPEX</i>	5
2.2 THE ROLE OF SOLVENT	7
2.3 MECHANISM	8
2.4 ANALYTICAL MODEL.....	9
2.5 EXPERIMENTAL APPROACH.....	11
2.6 NUMERICAL APPROACH.....	12
2.6.1 <i>Selection of the simulator</i>	13
CHAPTER 3	15
STATEMENT OF THE PROBLEM.....	15
CHAPTER 4	17
NUMERICAL SIMULATION	17
4.1 BACKGROUND	17
4.2 RESERVOIR FLUID CHARACTERIZATION	17
4.3 PVT DATA	20
4.4 EOS TUNING.....	23
4.4.1 <i>Tuning Parameters Other Than Viscosity</i>	24
4.4.2 <i>Viscosity Tuning</i>	26
4.4.3 <i>Generation of GEM EOS parameters</i>	27
4.5 SOLVENT SELECTION	28
4.5.1 <i>Injection Rate</i>	29
4.5.2 <i>Optimal Solvent</i>	30
4.5.3 <i>Solvent Effect on Heavy Oil</i>	33
4.6 NUMERICAL SIMULATION	35
4.6.1 <i>Reservoir Description</i>	35
4.6.2 <i>2D simulation settings</i>	37
4.6.3 <i>Initial Conditions</i>	39
CHAPTER 5	40
ANALYSIS OF SIMULATION RESULTS	40

5.1 OPTIMAL SOAKING TIME	40
5.1.1 <i>Three-month injection case</i>	40
5.1.2 <i>Six-month injection case</i>	41
5.1.3 <i>Nine-month injection case</i>	43
5.2 CYCLES DESIGN.....	44
5.3 NCSOR	45
5.4 COMPARISON OF SOAKING AND NO SOAKING CASES	47
5.4.1 <i>Simulation Results Comparison</i>	47
5.4.2 <i>What happens during the soaking period?</i>	49
5.4.3 <i>Solvent Left Behind</i>	55
5.5 COMPOSITIONAL ANALYSIS	55
5.6 WELL CONFIGURATIONS	57
5.7 RECOVERY FACTOR.....	61
CHAPTER 6	66
CONCLUSIONS AND SUGGESTIONS	66
REFERENCES	68
APPENDIX	74
APPENDIX 1. DATA FILE OF GEM	74

LIST OF TABLES

Table 1. C₃₀₊ compositional analysis	18
Table 2. Eight Pseudo-components	20
Table 3. Viscosity Profile	21
Table 4: Density Profile	21
Table 5. GOR and gas/liquid FVF data	23
Table 6. Regression Variables	24
Table 7. Regression Results	25
Table 8. Viscosity Regression Parameters	26
Table 9. Summary of Viscosity Regression Results	27
Table 10. Peng-Robinson EOS	28
Table 11. Component Properties	28
Table 12. Solvent Mixtures and their Dew Point Pressure	30
Table 13. Solvent Mixture Comparison	31
Table 14. Reservoir Description	36
Table 15. K_{rw} and K_{row} vs. S_w	37
Table 16. K_{rg} and K_{rog} vs. S_L	37
Table 17. 2D simulation settings	38
Table 18. Cycles Design	45
Table 19. NCSOR Comparison	46
Table 20. Schedule of the Production Cycles	50
Table 21. Compositional Analysis	56
Table 22. Sensitivity Analysis of Horizontal Distance (3,3,6)	58
Table 23. Sensitivity Analysis of Vertical Distance (3,3,6)	59
Table 24. Sensitivity Analysis of Horizontal Distance (3,3,6,6,6)	60
Table 25. Sensitivity Analysis of Vertical Distance (3,3,6,6,6)	61

LIST OF FIGURES

Figure 1. The Concept of the VAPEX Process⁸	3
Figure 2. WinProp interface window for Plus Fraction Splitting	19
Figure 3. Molecular Weight distribution of the Reservoir Fluid	19
Figure 4. Viscosity Profile of the Reservoir Fluid	22
Figure 5. Density Profile of the Reservoir Fluid	22
Figure 6. Dew Point Pressure of Solvent Mixture vs. C₁ Mole Fraction	31
Figure 7. Dissolved C₃ vs. C₁ mole fraction	32
Figure 8. Cum. oil vs. C₁ mole fraction	32
Figure 9. Ternary Plot at 5000 kPa, 21 °C	33
Figure 10. Ternary Plot at 8000 kPa, 21°C	33
Figure 11. Swelling Test	34
Figure 12. Two Phase Flash	35
Figure 13. K_{rw} and K_{row} vs. S_w	36
Figure 14. K_{rg} and K_{rrog} vs. S_L	36
Figure 15. Front View of the simulation settings	38
Figure 16. Viscosity Profile – 3-month Inj.	41
Figure 17. GOR Profile – 3-month Inj.	41
Figure 18. Viscosity Profile – 6 month Inj.	42
Figure 19. GOR Profile - 6 month Inj.	42
Figure 20. Cumulative Prod. – 6 month Inj.	43
Figure 21. Viscosity Profile - 9 month Inj.	43
Figure 22. GOR profile – 9 month Inj.	44
Figure 23. Cum. Prod. – 9 month Inj.	44
Figure 24. Production Comparison	47
Figure 25. GOR Comparison	47
Figure 26. Cumulative Production	48
Figure 27. Gas mole fraction (C_{1B}) at 2005-04-30, No-soaking	49
Figure 28. Gas mole fraction (C_{1B}) at 2005-08-30, Soaking	49
Figure 29. Gas mole fraction of C_{1B}, 1st Cycle	50
Figure 30. Gas Mole fraction of C_{1B}, 2nd Cycle	51
Figure 31. Gas Mole fraction of C_{1B}, 3rd Cycle	51
Figure 32. Gas mole fraction of C₃, 1st Cycle	52
Figure 33. Gas Mole fraction of C₃, 2nd Cycle	52
Figure 34. Gas Mole fraction of C₃, 3rd Cycle	52
Figure 35. Oil mole fraction of C_{1B} 1st Cycle	53
Figure 36. Oil Mole fraction of C_{1B}, 2nd Cycle	53
Figure 37. Oil Mole fraction of C_{1B}, 3rd Cycle	53
Figure 38. Oil mole fraction of C₃, 1st Cycle	54
Figure 39. Oil mole fraction of C₃, 2nd Cycle	54

Figure 40. Oil mole fraction of C₃, 3rd Cycle.....	54
Figure 41. Compositional Analysis	56
Figure 42. Front View of Well Configuration Parameters.....	57
Figure 43. Sensitivity Analysis of Horizontal Distance (3,3,6).....	58
Figure 44. Sensitivity Analysis of Vertical Distance (3,3,6).....	59
Figure 45. Sensitivity Analysis of Horizontal Distance (3,3,6,6,6).....	60
Figure 46. Sensitivity Analysis of Vertical Distance (3,3,6,6,6).....	61
Figure 47. Oil rate comparison cycles 3,3,6 and 3,3,6,6,6	63
Figure 48. 3D view of oil viscosity at the end of cycles 3,3,6.....	63
Figure 49. 3D view of oil viscosity at the end of cycles 3,3,6,6,6.....	64
Figure 50. 3D view of oil saturation at the end of cycles 3,3,6.....	64
Figure 51. 3D view of oil saturation at the end of cycles 3,3,6,6,6.....	65

LIST OF NOMENCLATURE

k = Cell permeability, (m^2)

g = Gravitational acceleration, (m/s^2)

ϕ = Porosity (fraction)

S_o = Mobile oil saturation (fraction)

h = Model height, (m)

$\Delta\rho$ = Density difference between solvent/oil mixture and the pure solvent, (kg/m^3)

C_s = Solvent concentration in the mixture (fraction)

D_s = Diffusion coefficient for the solvent in the mixture, (m^2/s)

μ = Viscosity of the mixture, (cp)

LIST OF ABBREVIATIONS

CCE = Constant Composition Expansion

CVD = Constant Volume Depletion

DL = Differential Liberation

EOS = Equation of State

FVF = Formation Volume Factor

NCSOR = Net Cumulative Solvent - Oil Ratio

OOIP = Original Oil in Place

SAGD = Steam - Assisted Gravity Drainage

SG = Specific Gravity

CHAPTER 1

INTRODUCTION

Due to the decline of the conventional oil reserves, the exploration of heavy oil and bitumen has become of primary interest to many oil companies.

Heavy oil resources in the world are estimated to be around one trillion m³, six times the conventional oil reserves, and might become a future potential source of energy¹. Canada is ranked second in terms of oil reserves, with an estimated OOIP of 400 billion m³, twice the total conventional oil deposits in the Middle East (Janisch²). Alberta has about 250 billion m³ heavy oil and oil sand deposits, buried at a depth of 0-800 meters; only 5% of the reserves are suitable for open-pit mining from shallow reservoirs³ (Wightman et al.⁴).

Successful extraction of this highly viscous crude oil poses a serious challenge to petroleum engineers. Since heavy oil has a lower economic value than conventional oil, it is more sensitive to fluctuations in oil prices and there is a tighter margin for a successful recovery method.

From previous studies^{5,6}, a recovery rate of only 3-10% can be currently achieved through primary recovery for a heavy oil reservoir. The second recovery method, flooding with water, is only applicable to moderately viscous oil reservoirs, such as those found in the Lloydminster area, where heavy oil has a viscosity ranging between 500-4000 cp. However, the incremental recovery rate is relatively low, due to the high adverse mobility ratio.

In order to produce from such heavy oil reserves, many traditional thermal recovery methods have been developed. These include: Steam-Assisted Gravity Drainage (SAGD), Cyclic Steam Stimulation, Steam Flooding, and in situ Combustion. However, because of the primary mechanism of these thermal techniques, steam has to be generated throughout the whole process and thus, many problems are raised with regard to fresh water resource shortage, water treatment difficulties, high pressure surface facility design, heat losses prevention, etc.

In order to compensate for the problematical reservoirs, because gas cap, bottom aquifer, low thermal conductivity, thin pay zone, high water saturation, low permeability (less than 1

Darcy), etc., are not suitable for steam based heavy oil recovery methods, the Vapor Extraction (VAPEX) process has been proposed by Butler and Mokrys⁷ as an alternative way of developing heavy oil reservoirs. In this process vaporized hydrocarbon solvents such as butane or propane are injected into the heavy oil reservoirs by a horizontal well and the solvent diluted oil is drained by gravity to the horizontal production well. Compared to its competitor processes, VAPEX is highly energy efficient, environmentally friendly, causes in-situ upgrading, and requires low capital investment⁷.

However, in the VAPEX process, the oil production rate in the field, as predicted by previous researchers, is too low to make this process attractive for field achievement. The contact area and contact time between solvent and heavy oil are very important in determining the oil production rate. Since the main mechanisms include solubilization of the solvent in oil, mass transfer from vapor to liquid phases by diffusion, reduction of oil viscosity by solvent dilution, and upgrading of the oil by asphaltene precipitation and deposition⁸, this study investigates the solvent soaking effect in order to maximize the mixing time and the contact area between the solvent and the heavy oil.

Most of the petroleum reservoirs in Alberta are 250 to 700 m deep; many are much deeper, because light hydrocarbon vapors only have a high solubility in oil when they are close to their dew point. A successful VAPEX design is more dependent on the prevailing reservoir pressure and temperature during production. In this thesis, the optimal solvent combination is obtained through dynamic simulation runs. Numerical studies of the VAPEX process are investigated based on the field scale with a horizontal permeability of 2 Darcy. The influences of solvent combination, solvent injection rate, solvent composition, soaking time, number of cycles, and well configuration are studied through numerical simulations with a compositional simulator.

CHAPTER 2

LITERATURE REVIEW

2.1 Vapor Extraction (VAPEX)

2.1.1 What is VAPEX?

The VAPEX process is emerging as an alternative method to the thermal recovery of heavy and extra heavy oils worldwide. The concept of VAPEX is very similar to that of SAGD. In VAPEX, vaporized light hydrocarbon solvent is injected into the reservoir and a vapor chamber, instead of a steam chamber, is formed around the horizontal injector; the solvent diffuses into the oil at the contact interface and the diluted, low viscosity oil drains by gravity towards the horizontal producer. At the point of higher solvent concentration, asphaltenes may precipitate and be left behind in the matrix. The well configuration during VAPEX usually consists of two parallel horizontal wells placed at the bottom layer of a reservoir, as shown in Figure 1. A few different well configurations are also possible. Applying horizontal wells maximizes the contact area between the solvent and reservoir fluid.

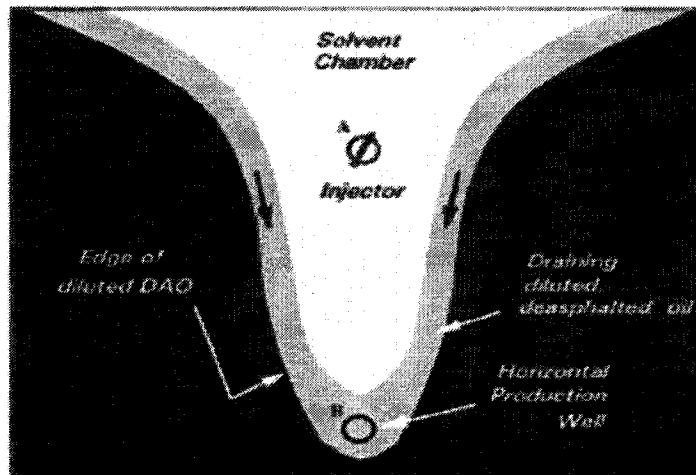


Figure 1. The Concept of the VAPEX Process⁸

Initially, the injected solvent vapor rises counter-currently with the draining diluted oil and

a rising vapor chamber is formed. Once the vapor chamber reaches the top of the reservoir, it spreads sideways until it encounters the pattern boundary. The process may still continue with a falling interface period until the rate becomes prohibitively low.

2.1.2 Why VAPEX?

The estimated worldwide heavy oil reserves are around six times those of conventional oil and might become an important energy resource in the future. Therefore, efficient recovery of heavy oil reservoirs has posed a challenge to the oil and gas industry, government organizations, and research institutes.

As the development of the traditional thermal recovery method proceeds, many problems have to be addressed, regarding either the character of the process itself, or the problematic reservoirs that are not suitable for thermal processes.

In comparison with SAGD, VAPEX is especially beneficial for thin pay zone reservoirs where the heat losses to the over- and under-burden have a negative impact on the performance of economics. The VAPEX process does not require water recycling and treatment, yields much lower carbon dioxide emissions and can be operated at reservoir temperature. The capital and operational costs are estimated to be much less than those of a SAGD project. The difference between the two projects could be summarized in the following points³:

- ✓ *Energy requirement:* The latent heat of propane is predicted to be 1/6 that of water⁷; to produce 1 kg of oil, 0.2-0.5 kg propane is needed, compared to the 3 kg of steam required in the thermal process. Thus, the energy consumed in VAPEX is 3% or less than that of SAGD;
- ✓ *Clay swelling:* Condensation of steam as water in SAGD may cause formation damage by clay swelling. Thus, for formations with a swelling clay content of more than 10%, SAGD is not recommended;
- ✓ *Aquifer Constrains:* Since solvent does not dissolve in water, the problem of energy loss in the SAGD process is much more severe than in VAPEX for reservoirs underlain

by aquifer;

- ✓ *Gas cap:* It is not suitable for VAPEX, because solvent escaping into the gas cap may adversely affect the economics of the process;
- ✓ *Upgrading Potential:* The VAPEX process has the potential to de-asphalt the crude oil if the solvent concentration is high enough. Thus, it may greatly reduce many downstream problems that will be encountered during transportation and refining.

In VAPEX, although the operating pressure is controlled by the reservoir pressure, solvent injection rate, and reservoir permeability, the operating temperature may be close to the reservoir temperature. This eliminates the need for thermal completions and reduces the operational cost. The volume of solvent injected is smaller than the volume of steam and thus the operating pressure would be lower in VAPEX. The surface facilities requirement for VAPEX, therefore, is much less expensive than for SAGD.

2.1.3 Difficulties with VAPEX

Since the diffusion and dispersion of solvent into the oil phase is an order of magnitude lower than the thermal diffusivity in the reservoir matrix, it is generally expected that the production rate in this solvent process will be much lower than in a steam process. This is due to the fact that the larger contact area between the solvent vapor and the crude yields a higher solvent mass transfer rate. In the VAPEX process, a pair of horizontal wells will usually be applied to maximize the contact region between the solvent agent and the crude oil.

In VAPEX it is very difficult to confine the vapor chamber; the solvent vapor losses may cause a serious problem and reflect on the economics of the process. However, steam escapes in a similar way but condenses in a short distance that hinders further losses. The problem of escaping solvent vapor is another main issue that delays the field application of this process.

The solvent pressure should be as close as possible to its vapor pressure at the reservoir temperature⁹. In field conditions, to avoid liquefaction of a solvent at any point in the reservoir, the pressure should be lower than the solvent's vapor pressure at the prevailing temperature.

Hence, the reservoir pressure and temperature play a significant role in the selection of the solvent. Because the vapor extraction solvent, propane or butane, usually has a low vapor pressure at the reservoir temperature, this may impose a serious limitation on the operating pressure and the applicability of the process in high-pressure reservoirs.

There are certain areas in VAPEX exploitation that are still under investigation and need further experimental work to be proven.

- *Role of capillary forces*¹: It was proposed that the capillary-induced countercurrent gas-liquid flow in the mixing zone could enhance the extraction rate. This needs to be confirmed through future lab studies. On the other hand, the capillary pressure works against the gravity head, which in turn will prevent the bottom layer of the reservoir from being drained. The portion of this un-drainable region depends on the capillary pressure and could become a significant negative factor in developing thin reservoirs of low permeability.
- *Heterogeneity of the reservoir*³: The shape of the vapor/steam chamber is controlled by reservoir heterogeneity, which includes oil sand thickness, facies changes, shale barriers, faults, fractures, and thief zones. High permeability thief zones or fractures may also change the natural progression of solvent vapor/steam in the reservoir as the vapor/steam preferentially moves along these streaks or fractures, thus evading the tighter surrounding matrix.
- *Asphaltene precipitation*: Previous study shows that asphaltene precipitation happens when the solvent composition exceeds the critical amount needed for the onset of de-asphalting for a specific situation¹⁰. Butler's experimental⁷ results showed that asphaltene precipitation occurred when the solvent concentration reached 35% by weight for extracting heavy oil with 15.6% weight percent of asphaltenes. Experiments performed by researchers from Total observed¹¹ that asphaltene flocculation started at a solvent mole fraction around 0.934. The precipitated asphaltenes can remain within the oil phase, or can deposit onto the rock surface. Thus, they may plug the formation and

alter the rock wettability (from water-wet to oil-wet)¹². Nevertheless, deposition of asphaltenes may also significantly reduce heavy oil viscosity and accelerate the oil flow rate.

In order to overcome the abovementioned difficulties, a successful VAPEX process needs to comprehensively consider key design criteria.

2.2 The role of Solvent

Usually, methane, ethane, propane, and butane are injected as the light hydrocarbon solvent during the VAPEX process. Light hydrocarbon vapors only have a high solubility when they are close to their dew point pressure. This requires that the reservoir pressure be close to their vapor pressure; if the reservoir pressure is higher than the solvent dew point pressure, the solvent vapor condenses and can not fill the cavity to maximize the contact area with the heavy oil. If the reservoir pressure is lower than the solvent dew point pressure, the vapor is under-saturated and can not dissolve into the oil phase effectively.

For example, the vapor pressure for ethane is about 3500 kPa, propane is about 800 kPa, and butane is about 190 kPa¹³ under a reservoir temperature close to room temperature. However, a lower reservoir pressure is hardly ever a problem; the pressure can usually be raised or a solvent with lower dew point pressure can be injected. Propane appears to be the best choice among those solvents, because propane has a 15% higher diffusivity and its vapor pressure is approximately four times higher than that of butane¹³. Furthermore, compared to ethane, it does not form two liquid phases with oil.

The amount of solvent used per barrel of produced oil will directly affect the economics of the extraction process. Results show¹⁴ that, for propane, a net cumulative solvent-oil ratio (NCSOR) of around 0.06-0.15 tons/tons maybe expected in practice, since the solvent in the reservoir is partially vaporized and partially dissolved. It is also predicted³ that in SAGD, with a steam-oil ratio (SOR) of 2.5 to 3, about 3 m³ of steam is used to produce 1 m³ of oil. On the other hand, in VAPEX, less than 1 m³ of liquid solvent under reservoir conditions is injected to

produce 1 m³ of oil.

As previous research indicates⁷, Canada produces about 50 million bbl/y (8 million m³/y) of pure propane, referred to as Liquefied Petroleum Gas (LPG), 80% of which comes from Canadian natural gas and 20% from by-products of crude oil.

The solvent-oil ratio would mainly depend on the solvent composition, oil properties, reservoir characteristics, and the operating conditions. Optimization of the solvent composition and the operating conditions is necessary on a case-specific basis.

2.3 Mechanism

The application of VAPEX to heavy oil recovery requires a confident prediction of the process' performance for a field scale operation. This, in turn, requires knowledge of the mechanisms at work in the process and the magnitude of each of these mechanisms.

The main mechanisms during a VAPEX process can be summarized according to previous experimental observations^{8,15,16,17}. In the first place, the solvent must diffuse into the oil phase for some time in the reservoir; this process can be numerically described by the diffusion coefficient parameter for a particular solvent and reservoir oil system. The solvent diffusion coefficient is a key value that governs the oil dilution efficiency, as well as the rate of production. The value of the diffusion coefficient depends on two dominant factors: convective dispersion and molecular diffusion, where the molecular diffusion is relatively small and may be important in the start-up phase when velocity is small. Once flow is established, the convective dispersion becomes the dominant driving force.

The diffusion coefficient depends on oil viscosity; the viscosity of the heavy oil will change drastically with the concentration of the dissolved gas and the potential for de-asphalting will further reduce the viscosity. As a consequence, the diffusion coefficient keeps changing at the edge of the vapor chamber, the region in which mass transfer takes place.

Secondly, after the solvent diffuses into the oil phase, the interfacial tension is reduced significantly, thus enabling the force of gravity to conquer the capillary pressure, so that the

diluted heavy oil can be drained towards the production well. This drainage is also aided by capillary imbibition⁸.

At the same time, the solvent dissolving into the oil phase can cause oil to swell^{3,17}. Increased liquid volume is a consequence of mixing the liquid solvent and the liquid oil; the swelling factor will also improve the oil drainage rate. Different solvents have different swelling factors under different pressure and temperature conditions.

In this thesis, the main mechanisms at work during the solvent extraction process will be further investigated through a numerical study.

2.4 Analytical model

Butler and Mokrys¹⁸ have developed an analytic model describing the VAPEX process by combining Fick's second law of diffusion, Darcy's equation, and the momentum balance. They assume that the mass transfer of solvent into bitumen occurs under pseudo steady state. They also assume that the solute-solvent interface moves at a constant speed in the x-direction.

In this model the estimated oil production rate is expressed by the following equation:

$$Q_b = 2L\sqrt{2kg\Delta S_o h N_s} \quad (1)$$

The multiplier 2 represents drainage from both sides of the vapor chamber, L is the length of the well, ΔS_o is difference between the initial and residual oil saturation, dimensionless and N_s is a dimensionless parameter which evolves with the effects of dispersive mixing. It has been defined in a complex way and depends on the intrinsic dispersion of the solvent.

$$N_s = \int_{c_{\min}}^{c=1} \frac{\Delta\rho D_s (1 - c_s)}{\mu} d \ln c_s \quad (2)$$

The quantities $\Delta\rho$, D_s and μ depend on the solvent fraction c_s . The lower limit of the integral, C_{\min} , is the minimum concentration of solvent required for mobilizing the crude, and has to be fixed arbitrarily. The upper limit of the integration variable, C is the interfacial concentration representing the solubility of gaseous propane in bitumen at the condition of temperature and pressure. This can be estimated from vapor-liquid equilibrium calculations, provided that the composition and critical properties of bitumen are available.

Butler and Mokrys conducted their experiments in a Hele-Shaw cell with Athabasca and Suncor bitumen, and toluene as solvent. The recovery rate from their experiment is well matched by their analytical model.

Boustani and Maini¹⁹ pointed out that the analytical value of N_s should be calculated based on an effective diffusivity rather than on the classical molecular diffusion coefficient. Butler and Mokrys' correlation does not account for dispersion effects, and thus overestimates the value of molecular diffusion and underestimates the mass transfer rate.

Karmaker, Maini and Yazdani^{20,21} claimed later in their research that Butler and Mokrys' model under-predicted the oil drainage rate by ignoring the effect of convective dispersion between the solvent and the virgin heavy oil. They proposed a new correlation to scale up the experimental data into real field cases and found that the convective dispersion depends on the drainage height and dominates the mass transfer mechanism. Their experimental results show that the drainage rate is a function of the drainage height to the power of 1.1-1.3, instead of the square root in Butler and Mokrys' results.

As a result of this study, the vertical space between the horizontal injector and producer, which is equivalent to the drainage height, does influence the overall production rate to a certain degree. However, there exists an optimal value for this parameter. In other words, in the field case, the drainage rate is not always positively proportional to the drainage height.

2.5 Experimental Approach

Many studies have been conducted on the laboratory scale in order to better understand phenomena occurring during this non-thermal, solvent-based heavy oil recovery process. These studies have focused on studying the role of the gas-oil ratio (GOR), different saturation pressures, vapor chamber temperature⁷, capillary pressure, asphaltene deposition and precipitation, reservoir heterogeneity^{1,8,11,22}, well geometry^{22,23,24}, reservoirs with aquifers or gas cap^{23,24} and diffusion coefficient^{10,15,16} in the VAPEX process.

The general and most representative results obtained from all the previous laboratory experiments could be summarized into several points:

- ✓ The temperature at the propane-oil interface will be increased by 4-6°C due to the latent heat released from the condensation of propane vapor. This will have a local effect; the system temperature will increase by 1°C and result in 2% higher oil recovery rate²⁴.
- ✓ Pressure cycling could be an advantage after the initial displacement phase because it promotes mixing and the formation of a free path for the diluted bitumen⁷.
- ✓ No asphaltene will precipitate unless the concentration of solvent reaches the critical level¹¹.
- ✓ Capillary pressure plays an important role in determining the overall drainage rate; it depends on interfacial tension, which is determined by the solvent dilution of the oil^{10,11}.
- ✓ The main mechanisms during the VAPEX process are gas-drive and the dilution effect of the solvent in heavy oil¹¹.
- ✓ The diffusion coefficient, as a parameter to model the VAPEX process analytically, is a key factor to controlling the mass transfer rate. It is the sum of convective dispersion and molecular diffusion, the later having much less influence. It varies with changes in oil viscosity during the whole process^{10,15,16}.
- ✓ The presence of a gas cap is found to be compatible for the VAPEX process; in this situation, a higher initial gas injection rate is preferred²⁴.
- ✓ Reservoirs with aquifer will promote the counter-current extraction rate if the horizontal

injector and producer are placed at the oil-water interface²³.

There are certain application limitations for the above results. Most of the models are made from phenolic resins⁷, glass beads, and unconsolidated or consolidated sand packs^{10,15,16}, and have permeability ranging from 5 to 200 Darcy, or even higher. For instance, the Hele-Shaw cell experiments developed by Butler and Mokrys^{7,8} use the concept of capillary bundles, which is different from the capillary effect in porous media, and results in a zero residual oil saturation, which would never happen in the field. Therefore, conclusions resulting from an analysis of their experimental observations are not accurate enough to represent what will happen during solvent extraction in real field cases.

The motivation for using typical permeability on the field scale is illustrated through this simulation study. Their experimental results are also re-evaluated at the end.

2.6 Numerical Approach

Most of the numerical simulation work has been done with the aim of investigating several important mechanisms involved in a solvent-based heavy oil recovery process: (1) mass transfer by convective dispersion and molecular diffusion at the contact interface between solvent and reservoir fluid, (2) asphaltene precipitation.

The performance of the VAPEX process is directly related to the amount of solvent dissolved into the heavy oil. Mass transfer of the solvent at the leading boundary is the key factor in the overall process. Diffusion and dispersion are the parameters controlling mass transfer at the leading front.

Nghiem²⁵ developed an equation of state compositional model where molecular diffusion and convective dispersion are incorporated into the mass balance. A constant dispersivity coefficient is used as a direct multiplier to the phase velocity. He advocated that the mixing mechanism is controlled primarily by the total dispersion coefficient. On the other hand, Perkins and Johnston²⁶ presented the relationships for predicting the total mass transfer under the influence of longitudinal and transverse dispersions, which consider both diffusion and dispersion

components.

There are several theories for the estimation of the diffusion coefficient in the literature^{27,28,29}. Hayduk and Minhas²⁶ presented a correlation for the estimation of the molecular diffusion coefficient of paraffin solute/solvent pairs as a function of temperature, molar volume of the solvent (propane), and viscosity of the medium within which diffusion is occurring. Compared to other methods, their model yields the smallest average deviation from the experimental results.

Nghiem, Kohse, and Sammon introduced a method for simulating asphaltene precipitation^{25,30,31,32}. The key theory of modeling asphaltene precipitation involves splitting the heaviest component in the study oil into a non-precipitating component, C_{31A+}, and a precipitating component, C_{31B+}. These two components have identical critical properties and acentric factors, but different interaction coefficients with the light components³², the latter having a higher interaction coefficient value.

2.6.1 Selection of the simulator

GEM³³ and STARS,³⁴ developed by the Computer Modeling Group, are compared here in order to select an appropriate simulator for solvent based heavy oil recovery processes. GEM uses an equation of state (EOS) to model fluid phase behavior and predict fluid properties, such as density, viscosity, and volume shift. This is a more accurate and flexible approach than the STARS equilibrium K-tables. GEM can accurately predict K-values (for phase split) and z-factor for fluid densities. The K-value is the ratio of mole fraction of a component in the gas phase to mole fraction in the liquid phase. STARS does not use EOS because it would be too numerically expensive in non-isothermal conditions. Instead, K-values are given in a table usually generated by WinProp³⁵. That is why GEM is more capable of modeling complex phase changes like asphaltene precipitation and miscibility than STARS.

On the other hand, the advantage of STARS is the modeling of thermal effects. It may be important in some cases when steam injection precedes solvent injection. STARS can model both stages, but the PVT predictions are not as good as in GEM.

GEM needs more PVT data than STARS. The key experimental data needed in GEM are the reservoir fluid analyses: composition, standard experiments of constant composition expansion (CCE), constant volume depletion (CVD) and separator test. All these data can be used with WinProp to generate and tune the EOS parameters for running GEM.

CHAPTER 3

STATEMENT OF THE PROBLEM

One of the major challenges presented by the solvent-based heavy oil recovery method is the unattractive oil drainage rate, which is determined by molecular diffusion and convective dispersion mechanisms. This is also the main reason for the reluctance to apply VAPEX in the field; the production performance will directly influence the process economics. In order to promote a faster mass transfer, the cyclic solvent soaking effect is investigated and the results are illustrated through a comparison of the NCSOR¹² of no soaking and optimally designed soaking cases.

The concept of Cyclic Solvent Soaking is very similar to that of Cyclic Steam Stimulation (CSS) - instead of soaking the injected steam, the solvent vapor is injected into the reservoir and soaked for an appropriate amount of time. During this soaking period, more solvent will diffuse into the oil phase and dissolve into it. Thus, the viscosity of the heavy oil that is close to the vapor chamber will be reduced and, once it reaches a removable, low viscosity, level, it will flow to the horizontal producer under the force of gravity. Following that, more viscous oil will be exposed and come into contact with the expanding solvent along the vapor chamber and the process will continue. The production stage will follow directly after the solvent injection and soaking period for one cycle. Then, more cycles will be designed to produce more oil.

Another important criterion regarding the solvent-based heavy oil recovery method is the solvent selection. As mentioned in the section 2.2, the dew point pressure of an effective solvent candidate has to be close to the prevailing reservoir pressure during the whole process. By applying this criterion, the solvent will contain some gas as well as some liquid. The purpose of the presence of the gas is to carry the effective liquid solvent and maximize the contact area between the solvent and the reservoir oil. On the other hand, the liquid solvent, as a more aggressive element, will significantly reduce the viscosity of the heavy oil in-situ if the

concentration reaches a critical value.

Most of Alberta's reservoirs are around 250-500 m in depth; pure propane has been used as a solvent wherever VAPEX has been tried. Before the propane reaches the reservoir, it is already liquefied. In order to apply VAPEX to some high-pressure reservoirs, an appropriate solvent mixture needs to be developed. Methane, ethane, and propane are selected as a solvent pool and different combinations of these three substances are examined and compared through dynamic simulations. Finally, the most effective solvent mixture is determined for further study.

A compositional simulator is chosen to perform the simulation studies. A detailed analysis of the composition of the reservoir fluid before and after simulation can be conducted with this compositional simulator. Meanwhile, the amount of each individual solvent consumed in the solvent mixture can be tracked and recorded for different cycles.

CHAPTER 4

NUMERICAL SIMULATION

4.1 Background

The reservoir fluid used in the study was a recombination of methane and Lloydminster-type dead oil. The oil sample was sent to a commercial laboratory for analysis. The process of PVT data analysis included: recombination of C_1 at standard conditions to a GOR of 15 sm^3/sm^3 ; C_{30+} composition of the recombined fluid sample; saturation pressure of the recombined fluid at room temperature; density and viscosity of the recombined fluid at bubble point pressure, and at three points below the bubble point pressure at room temperature; EOS modeling for single stage flash; prediction of GOR and gas/liquid Formation Volume Factor (FVF) data.

4.2 Reservoir Fluid Characterization

The C_{7+} fraction of an oil sample contains hundreds or thousands of individual chemical constituents. Heavy end component characterization refers to the process of describing all of these components as one or several pseudo-components. Each of the pseudo-components will have a defined critical temperature, critical pressure, acentric factor, and binary interaction coefficient so that it can be used with the EOS. A number of publications^{36,37,38} emphasize C_{7+} characterization as the key element in attaining agreement between EOS and laboratory results.

The C_{30+} composition analysis listed in Table 1 shows the molecular weight and mole percent of each individual hydrocarbon component in both the dead oil sample and the recombined reservoir fluid. The molecular weight and specific gravity of C_{7+} are 487.2 and 0.9811, respectively. With the extended analysis³⁵ data, the C_{7+} components were lumped into three pseudo-components: C_7-C_{23} , $C_{24}-C_{33}$, and C_{33+} by the "Plus Fraction Splitting" icon in WinProp (Figure 2). The molecular weight distribution of the components follows the 2-stage

exponential distribution (Figure 3); the critical properties of each pseudo-component were calculated with the Twu³⁵ correlation by using the mixing rule.

Table 1. C₃₀₊ compositional analysis

No.	Component	Flashed- Wt %	Mono- Wt %	Fluid Mole %	No.	Component	MW g/mol	Oil Mole %	Fluid Mole %
1	C1	0.000	0.993	23.288	21	C11	147	2.018	1.548
2	C2	0.000	0.000	0.000	22	C12	161	2.504	1.921
3	C3	0.001	0.001	0.008	23	C13	175	3.493	2.680
4	i-C4	0.001	0.001	0.008	24	C14	190	3.845	2.950
5	n-C4	0.001	0.001	0.006	25	C15	206	4.223	3.240
6	i-C5	0.004	0.004	0.020	26	C16	222	3.958	3.036
7	n-C5	0.003	0.003	0.016	27	C17	237	3.833	2.940
8	C6	0.045	0.044	0.198	28	C18	251	3.532	2.710
9	Mcyclo-C5	0.009	0.009	0.039	29	C19	263	3.420	2.624
10	Benzene	0.000	0.000	0.000	30	C20	275	3.165	2.428
11	Cyclo-C6	0.010	0.009	0.042	31	C21	291	2.978	2.285
12	C7	0.067	0.067	0.250	32	C22	300	2.485	1.906
13	Mcyclo-C6	0.032	0.032	0.123	33	C23	312	2.452	1.881
14	Toluene	0.003	0.003	0.012	34	C24	324	2.231	1.711
15	C8	0.110	0.109	0.384	35	C25	337	2.070	1.588
16	C2-Benzene	0.009	0.009	0.030	36	C26	349	1.918	1.471
17	m&p-Xylene	0.011	0.011	0.040	37	C27	360	1.962	1.505
18	o-Xylene	0.012	0.012	0.042	38	C28	372	1.673	1.284
19	C9	0.152	0.151	0.468	39	C29	382	1.860	1.427
20	C10	0.370	0.366	1.028	40	C30+	800	42.839	32.863

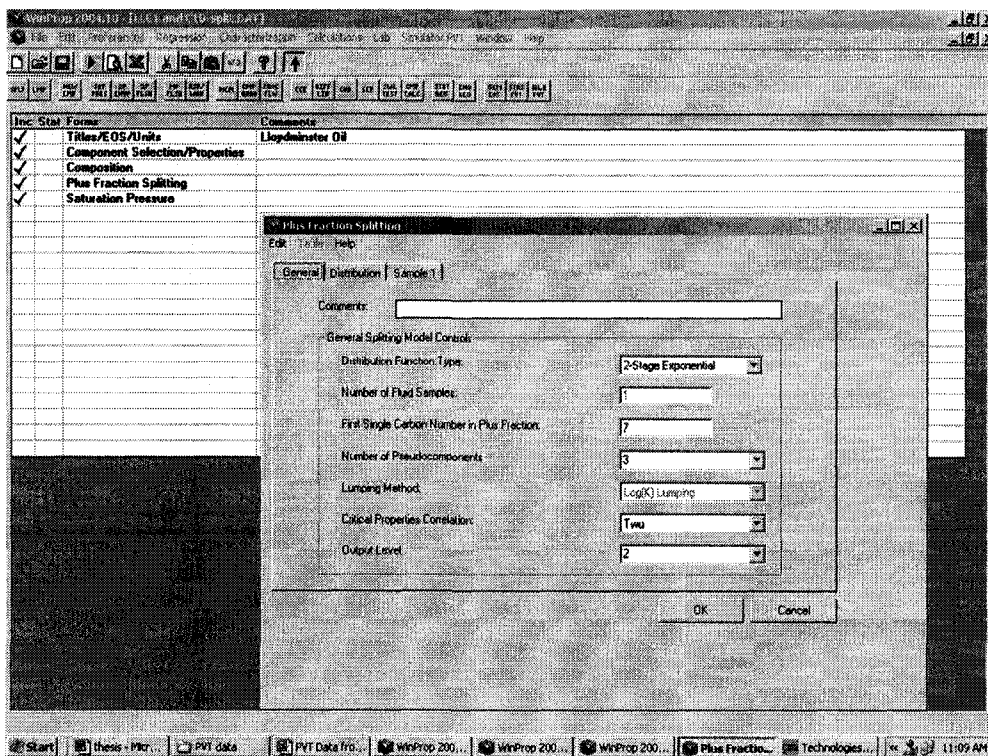


Figure 2. WinProp interface window for Plus Fraction Splitting

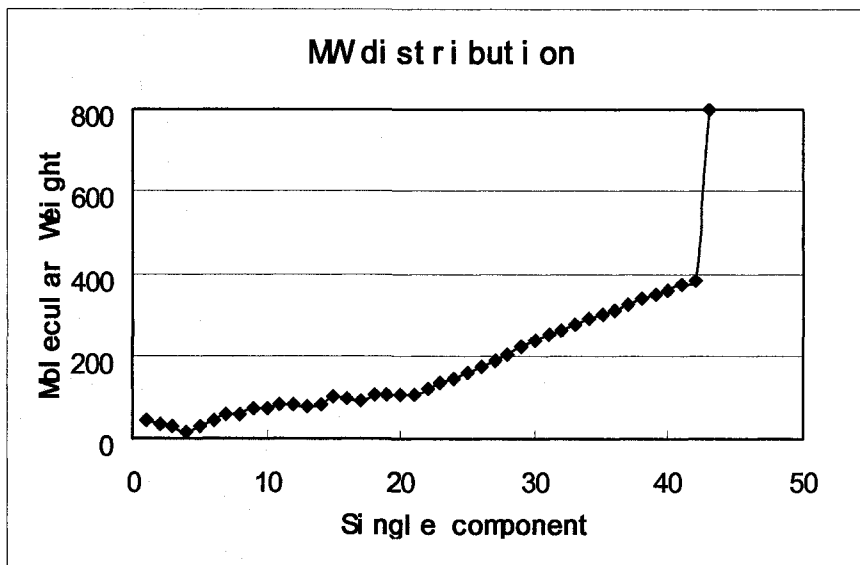


Figure 3. Molecular Weight distribution of the Reservoir Fluid

In the end, the reservoir fluid is described in terms of a total of eight pseudo-components (Table 2). As required, C_1 , C_2 , and C_3 have to be maintained as individual components to account for the solvent. In addition, C_{1B} is defined with the same critical properties as C_1 in

order to distinguish the injected methane from the original methane that was recombined with the Lloydminster dead oil sample. The eight pseudo-components are tabulated in Table 3.

Table 2. Eight Pseudo-components

No.	Component	Composition (mole fraction)	MW	SG
1	C ₁	23.30%	16.04	0.300
2	C _{1B}	0.00%	16.04	0.300
3	C ₂	0.000%	30.07	0.356
4	C ₃	0.008%	44.10	0.507
5	IC ₄ -NC ₆	0.330%	83.23	0.679
6	C ₇ -C ₂₃	28.45%	208.4	0.845
7	C ₂₄ -C ₃₂	15.05%	331.5	0.904
8	C ₃₃₊	32.86%	800.0	1.035

In Table 2, components IC₄ to NC₆ are lumped into one pseudo-component, due to their similar properties. C₁ makes up 23% of the recombined oil, and C₃₃₊ almost 33%.

4.3 PVT data

The live oil viscosity measured at the saturation pressure and a temperature of 21°C is 2941 cp. The saturation pressure of the recombined reservoir fluid is 4068 kPa; after flashing to the surface conditions, a GOR of 14.56 sm³/sm³ is obtained. The density of the reservoir fluid at standard conditions is 0.984 g/cm³, and the API gravity at standard conditions is 12.27°. The molecular weight is calculated as 485.4 using the mixing rule.

The viscosity values at various pressure levels and a constant temperature of 21°C were measured and the results are shown in Table 3. The density results at different pressures and the same constant temperature were also measured and are listed in Table 4.

Table 3. Viscosity Profile

	Pressure kPa	Pressure psia	Viscosity cp
	20684	3000	5105
	13790	2000	4088
	9653	1400	3490
	6895	1000	3097
Pb	4068	590	2941
	4068	590	2941
	1379	200	8383
	103	15	12895

Table 4: Density Profile

	Pressure kPa	Pressure psia	Density g/cc	API
	13787	2000	0.982	12.59
	13091	1899	0.981	12.73
	12395	1798	0.980	12.86
	11705	1698	0.979	12.99
	11009	1597	0.979	13.08
	10306	1495	0.978	13.23
	9644	1399	0.976	13.46
	8947	1298	0.975	13.60
	8251	1197	0.974	13.81
	7906	1147	0.973	13.86
	7555	1096	0.973	13.99
	7217	1047	0.972	14.10
	6893	1000	0.971	14.19
	6548	950	0.970	14.31
	5852	849	0.968	14.61
	5500	798	0.967	14.78
Pb	4068	590	0.963	15.44
	2758	400	0.968	14.68
	1379	200	0.973	13.93
	689	100	0.978	13.18
	101	14.7	0.982	12.67

From Figure 4, one can see that the viscosity at the surface condition of 1 atm is equal to the dead oil viscosity of 12,895 cp. As the pressure is increased, the viscosity is significantly reduced as more methane is dissolved into the oil. The viscosity of the reservoir fluid reaches the lowest point at 2941 cp, with a saturation pressure of 4068 kPa; the oil system is then saturated with methane. When the pressure is increased beyond the saturation pressure, the viscosity increases slowly.

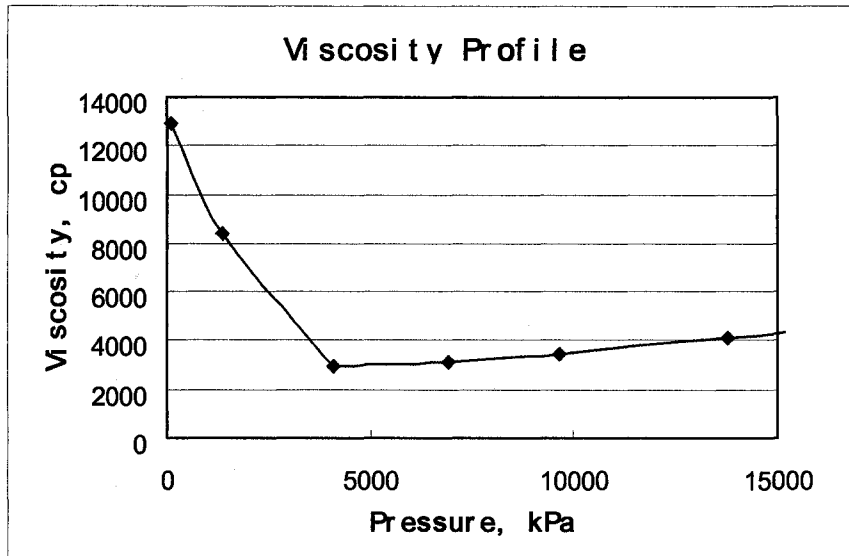


Figure 4. Viscosity Profile of the Reservoir Fluid

Figure 5 shows the density profile of the reservoir fluid. It has a trend similar to that of the viscosity profile: the density first decreases with an increase in pressure up to the saturation pressure, and then increases as the pressure increases beyond the saturation pressure. The density reaches the lowest value at the saturation pressure. The entire measurement was performed at a constant temperature of 21°C.

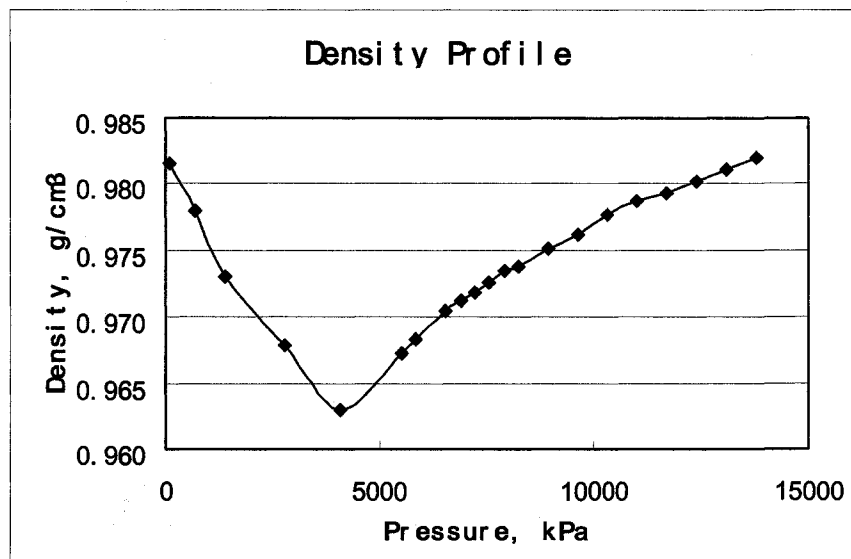


Figure 5. Density Profile of the Reservoir Fluid

In addition, other properties such as the oil formation volume factor (FVF), gas specific gravity (SG), gas viscosity, and GOR values were also recorded below the saturation pressure at a temperature of 21°C, and are tabulated in Table 5.

Table 5. GOR and gas/liquid FVF data

	Pressure kPa	Pressure psia	Density g/cc	Bo bbl/stb	Gas SG air=1	Gas Visc cP	GOR/step m ³ /m ³
Pb	4068	590	0.961	1.031			14
	2758	400	0.968	1.021	0.5539	1.16E-02	9.1
	1379	200	0.974	1.01	0.5540	1.13E-02	4.25
	689	100	0.978	1.005	0.5543	1.12E-02	1.92
	101	14.7	0.98	1.001	0.5567	1.11E-02	0

4.4 EOS Tuning

It is well known that a cubic equation of state (EOS)³⁶ will not generally accurately predict laboratory data for oil/gas mixtures without the EOS parameters being tuned (Coats and Smart³⁹). The objective function of the regression involves the solution of complex nonlinear equations, such as flash and saturation-pressure calculations. A robust minimization method is therefore required for rapid convergence to the minimum. In WinProp³⁶, a modification of the adaptive least-squares algorithm of Dennis et al.⁴⁰ is used.

It should be stressed that the regression procedure will not correct the deficiencies of the EOS used, and the EOS predictive capability depends entirely on the type and accuracy of the data used in the regression. For predictive purposes, attempts should be made to ensure that the “tuned” parameters are within reasonable physical limits.

Normally, regression parameters such as critical pressure, critical temperature, acentric factor, etc. of the heavy end components can be adjusted to tune the EOS. Specifically, the binary hydrocarbon interaction coefficients are the practical parameters that can be used to tune the saturation pressure. To modify densities and Z-factors, volume shift is the target parameter, which needs to be adjusted.

Another feature, which is especially important for heavy oil property tuning is the viscosity regression. It is modified separately from all the other properties, and the viscosity correlation

coefficients are the target tuning parameters. For predicting heavy oil viscosity, the Pedersen correlation usually gives better results than does the Jossi-Stiel-Thodos (JST) correlation³⁵. In the Pedersen correlation, the viscosity of the fluid depends on the components' critical temperatures and critical pressures; in contrast, in the JST correlation, the viscosity of the fluid depends more on phase molar volume.

4.4.1 Tuning Parameters Other Than Viscosity

For tuning the EOS of the studied reservoir fluid, the following parameters were picked as the regression parameters: the hydrocarbon binary interaction coefficient exponent, the critical pressure and critical temperature of the heaviest component, C_{33+} , and the volume shift parameters for the pseudo-components C_7-C_{23} , $C_{24}-C_{32}$ and C_{33+} . The specified regression variables are listed in Table 6.

Table 6. Regression Variables

Variable	Component Name	Initial Value	Lower Bound	Upper Bound	Final Value	Percent Change %
PVC3		1.20	0.00	1.80	0.00	-100
PC	C_{33+}	6.88	5.50	10.16	5.87	-14.63
TC	C_{33+}	1143.2	1002.6	1371.8	1068.5	-6.53
SH	$C_{07-C_{23}}$	0.15	0.10	0.25	0.10	-34.04
SH	$C_{24-C_{32}}$	0.13	0.08	0.30	0.08	-39.24
SH	C_{33+}	0.05	-0.15	0.40	0.37	748.84

Legend:

PVC3 - Parameter for HC-HC interaction coefficient exponent

PC - Critical pressure (atm)

TC - Critical temperature (K)

SH - Volume shift (dimensionless)

As a result, PVC3 was adjusted from 1.2 to 0; PC and TC had the smallest percent change before and after regression. The volume shift value for C_{33+} was tuned from 0.05 to 0.37, which means the original EOS gave a poor prediction of C_{33+} density. After tuning the EOS, the density value of C_{33+} was adjusted to match the experimental data. Generally, volume shift has

a wider range to match; the upper and lower boundaries can go anywhere beyond 70%.

All the available experimental PVT data are included in the regression calculation: saturation pressure, differential liberation data, and density and viscosity at different pressure levels. With the exception of viscosity, all these available experimental data should be matched at one time. The regression results are summarized in Table 7.

Table 7. Regression Results

Data Type	Pressure kPa	Experimental Data	Before Regression	After Regression	Error Reduction %	Error After %	Weight Factor
PSAT		4068	7821	4070	92.21%	0.05%	10.0
ROV	4068	1.03	1.025	1.033	0.35%	0.23%	1.00
	2758	1.02	1.010	1.022	0.98%	0.13%	1.00
	1379	1.01	1.005	1.011	0.35%	0.12%	1.00
	689	1.01	1.003	1.006	0.10%	0.09%	1.00
	101	1.00	1.001	1.002	0.10%	0.06%	1.00
GOR	4068	13.99	11.860	14.260	13.30%	1.93%	1.00
	2758	9.11	4.201	9.262	52.14%	1.72%	1.00
	1379	4.25	2.027	4.310	50.88%	1.42%	1.00
	689	1.92	0.934	1.951	49.81%	1.55%	1.00
DL	4068	0.96	0.798	0.961	16.91%	0.18%	1.00
	2758	0.97	0.805	0.968	16.75%	0.04%	1.00
	1379	0.97	0.808	0.976	16.73%	0.28%	1.00
	689	0.98	0.809	0.979	17.20%	0.12%	1.00
	101	0.98	0.810	0.982	17.55%	0.02%	1.00
API		12.27	43.107	12.344	250.68%	0.59%	1.00
DR		0.98	0.810	0.984	17.61%	0.05%	1.00

Legend:

PSAT: Saturation pressure

ROV: Reservoir oil formation volume factor

GOR: Gas-oil ratio

DL: Differential liberation data for oil specific gravity

API: Oil API gravity at standard conditions

DR: Oil specific gravity at standard conditions

DR: Oil Specific Gravity at Standard Conditions

In Table 7, the experimental data, values before and after regression are compared. The improvement in the EOS is demonstrated through the error after regression. The weight factor

indicates the weight of the importance of the experimental data. Usually saturation pressure has a high weight factor; here a weight number of 10 was determined during the regression procedure.

Examining the column showing the error after regression indicates that the differences between the actual experimental data and the simulation results predicted by WinProp are approximately 0.1% to 0.2%. For GOR matching results, the error is 1.4%-1.9%. The accuracy of these values is acceptable.

4.4.2 Viscosity Tuning

There are two choices available in WinProp and GEM for making viscosity correlations: Jossi-Stiel-Thodos (JST) and Pederson. Both of these options give good predictions of gas viscosity. Conversely, in order to predict liquid viscosities, their correlation coefficients should be fitted to the experimental data. JST is computationally much cheaper than Pederson, but Pederson may give better predictions for petroleum liquids with viscosities up to 6 cp, and will allow variations in the modeling of heavy oil viscosity with temperature and solvent concentration.

For the JST correlation, viscosity is more sensitive to phase molar volume, and for the Pederson correlation, viscosity depends on component critical temperature and critical pressure, as well as the coefficients b_i ($i = 1-5$). These five coefficients are used and adjusted to match the experimental data. Table 8 lists the initial and final values of the regression parameters and their corresponding upper and lower bounds and the percentage change.

Table 8. Viscosity Regression Parameters

Variables	Lower Bound	Upper Bound	Initial Value	Final Value	% Change
MU 1	0.0001	0.00016	0.00013	0.00010	-23.31
MU 2	1.842	2.764	2.303	2.510	9
MU 3	0.0059	0.0089	0.0074	0.0089	20
MU 4	1.478	2.216	1.847	1.855	0.41
MU 5	0.414	0.621	0.517	0.414	-20

The upper bound and lower bound default values are usually taken as $\pm 20\%$ of the initial value.

Table 9. Summary of Viscosity Regression Results

Data Type	Pressure kPa	Experimental Data	Before Regression	After Regression	Error Reduction	Error After	Weight Factor
MUL	4068	2941	44892	2866	14.2	2.54%	1.00
	1379	8383	505860	8553	59.3	2.03%	1.00
	101	12895	1764400	12910	135.8	0.12%	1.00

According to the results in Table 9, errors after regression were reduced significantly to around 2%, which is acceptable. For higher accuracy, the lower and upper bounds could be adjusted to a slightly wider range, or a greater weight factor could be applied. But generally, with the tuning viscosity weight factor set to 1.0, the error after regression is small enough.

4.4.3 Generation of GEM EOS parameters

GEM uses exactly the same EOS and thermodynamic model as WinProp. In GEM, only two hydrocarbon fluids phases are allowed, in addition to water and the optional solid phase. The EOS parameters for each component generated by WinProp are tabulated in Table 10. To facilitate comparison, properties of the individual components are listed in Table 11. All the EOS parameters and properties of the individual components will be output to a GEM data file in the reservoir fluid session.

Table 10. Peng-Robinson EOS

	C ₁	C _{1B}	C ₂	C ₃	IC ₄ -C ₆	C ₇ -C ₂₃	C ₂₄ -C ₃₂	C ₃₃₊
Omega A	0.457	0.457	0.457	0.457	0.457	0.457	0.457	0.457
Omega B	0.0778	0.0778	0.0778	0.0778	0.0778	0.0778	0.0778	0.0778
Vc for viscosity	0.099	0.099	0.148	0.203	0.336	0.753	1.105	2.075
Parachor	77.00	77.00	108.00	150.30	244.77	566.11	817.50	1164.60
Rackett Const, Zra	0.288	0.288	0.279	0.276	0.272	0.256	0.249	0.213
Vol Shift/b	-0.154	-0.154	-0.102	-0.073	-0.010	0.097	0.077	0.365
Vol Shift, m ³ /kmol	-0.0041	-0.0041	-0.0041	-0.0041	-0.0009	0.0237	0.0304	0.4244
EOS bc, m ³ /kmol	0.027	0.027	0.040	0.056	0.097	0.244	0.392	1.162
EOS Cappa Term	0.387	0.387	0.523	0.603	0.767	1.163	1.512	2.214

Table 11. Component Properties

	C ₁	C _{1B}	C ₂	C ₃	IC ₄ -C ₆	C ₇ -C ₂₃	C ₂₄ -C ₃₂	C ₃₃₊
Sg	0.300	0.300	0.356	0.507	0.679	0.845	0.904	1.035
Tb,	111.70	111.70	184.50	231.10	333.18	543.39	665.95	999.20
Pc, atm	45.40	45.40	48.20	41.90	32.75	19.02	13.77	5.87
Vc, m ³ /kmol	0.099	0.099	0.148	0.203	0.336	0.753	1.105	2.075
Tc, deg K	190.60	190.60	305.40	369.80	499.12	727.84	846.38	1068.55
Zc	0.287	0.287	0.285	0.280	0.268	0.240	0.219	0.139
Acentric	0.008	0.008	0.098	0.152	0.267	0.560	0.833	1.428
Molecular Weight	16.04	16.04	30.07	44.10	83.23	208.37	331.45	800.00

4.5 Solvent Selection

As discussed in the previous chapter, the criterion for selecting the optimal solvent is the dew point pressure of the solvent mixture. The dew point pressure has to be close to the prevailing reservoir pressure. The reason for this is that, when the solvent mixture is around the dew point pressure, there is enough gas to maximize the contact area between the solvent and the reservoir fluid. The gas will carry the liquid solvent and transport it through the porous medium. At the same time, there is also a certain amount of liquid in the solvent that will dissolve into the reservoir fluid to reduce the viscosity. Thus, the viscous heavy oil becomes mobile and drains

towards the production well.

The selection of the optimal solvent depends on some critical background information, which includes the particular reservoir type being studied; properties such as initial pressure, permeability, porosity; injection rate, as different injection rates will result in different prevailing pressures during the whole cyclic soaking process; and properties of the reservoir fluid, such as viscosity, density, component, component composition. Since all the properties of either the reservoir or the reservoir fluid are fixed, the only variable is the injection rate. The next section outlines how to choose the injection rate.

4.5.1 Injection Rate

Generally, the solvent injection rate should be designed based on the final results of an economic analysis. In this analysis, the net cumulative solvent-oil ratio (NCSOR) is one of the main economic evaluation criteria. Later on in the thesis, the NCSOR value is reported as a reference value in evaluating the three simulation cases. On the other hand, since solvent injection is an extremely high-pressure process, in order to prevent the reservoir from being fractured, the pressure distribution profile throughout the reservoir needs to be monitored during the entire process. This, in turn, limits the solvent injection rate.

Different solvent injection rates, ranging from 2000 to 4500 m³/day, were tested and compared in the simulation work. The simulation results indicated that, within this range, the higher the solvent injection rate, the more enhanced the cumulative oil production rate. However, because of pressure constraints, an injection rate of 4500 m³/day was found to be appropriate. At this injection rate, the prevailing pressure during the whole process was around 4500-8000 kPa, which is acceptable based on a formation fracture pressure of 10,000 kPa.

During the injection period, the pressure built up quickly because of the small reservoir permeability, 2 Darcy for the horizontal direction and 1 Darcy for the vertical direction, and the high injection rate. During the soaking period, the pressure decreased to a certain level, and during the production stage, the pressure decreased even further.

4.5.2 Optimal Solvent

C_1 , C_2 , and C_3 at different concentration levels were mixed in order to search for the best solvent combination. At a temperature of 21°C, the saturation pressure of pure C_2 is 3,872 kPa, and that of pure C_3 , 858 kPa. Since the critical temperature for C_1 is less than 21°C, it is gaseous at all times, regardless of the pressure conditions.

In order to keep the dew point pressure at around 6000 kPa, based on the prevailing reservoir pressure of 4000 to 8000 kPa, the solvent mixture has to contain a certain amount of C_1 to raise the dew point pressure level. Meanwhile, as C_3 has the highest solubility among the three solvents, it will assume the most responsibility for reducing the viscosity of the reservoir oil. A sufficient amount of C_3 has to be guaranteed. Based on the above discussion, the dew point pressures of different solvent mixtures were computed and are tabulated in Table 12. A starting point for the C_1 mole fraction was 0.3. In addition, the C_1 mole fraction and the corresponding dew point pressure are given in Figure 6.

Table 12. Solvent Mixtures and their Dew Point Pressure

No.	Solvent Composition (mole fraction)	Dew Point Pressure (kPa)
1	0.3 C_1 + 0.7 C_3	5510
2	0.3 C_1 + 0.2 C_2 + 0.5 C_3	5968
3	0.32 C_1 + 0.1 C_2 + 0.58 C_3	6041
4	0.34 C_1 +0.66 C_3	6122
5	0.36 C_1 +0.64 C_3	6430
6	0.38 C_1 +0.62 C_3	6740
7	0.39 C_1 +0.61 C_3	6892
8	0.4 C_1 + 0.6 C_3	7044
9	0.42 C_1 + 0.58 C_3	7343
10	0.5 C_1 + 0.5 C_3	8463

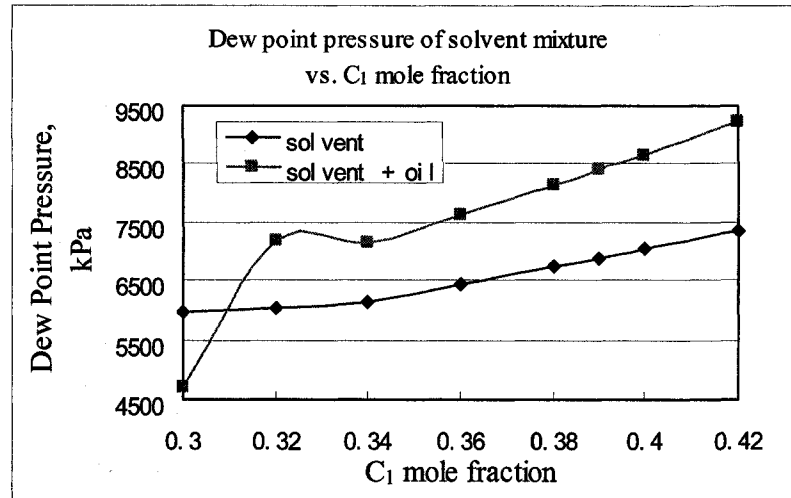


Figure 6. Dew Point Pressure of Solvent Mixture vs. C₁ Mole Fraction

As shown in Table 12, the higher the concentration of C₁, the higher the dew point pressure of the mixture. Taking out the first and last solvent mixtures, corresponding to the lowest and highest dew point pressures, gives the solvent mixtures used for 1 cycle simulation. The cumulative oil production, and dissolved C₁ and C₃ in the produced oil were computed and are listed in Table 13.

Table 13. Solvent Mixture Comparison

No.	Solvent composition mole fraction	P _{sat.} kPa	Swelling test (solvent+oil) kPa	Cum. Oil m ³	Disolved Solvent in Produced Oil, kg		
					C ₁	C ₂	C ₃
2	0.3 C ₁ + 0.2 C ₂ + 0.5 C ₃	5968	4700	3138	451	13195	983
3	0.32 C ₁ + 0.1C ₂ + 0.58 C ₃	6041	7180	3539	505	17593	571
4	0.34 C ₁ + 0.66 C ₃	6122	7170	3954	567	23279	-
5	0.36 C ₁ + 0.64 C ₃	6430	7640	8730	1010	67433	-
6	0.42 C ₁ + 0.58 C ₃	7343	9220	10083	1016	87717	-
7	0.4 C ₁ + 0.6 C ₃	7044	8660	10830	1096	93873	-
8	0.38 C ₁ + 0.62 C ₃	6740	8140	11000	1137	93850	-
9	0.39 C ₁ + 0.61 C ₃	6892	8400	11091	1134	95401	-

The swelling test is a function built into WinProp; the saturation pressure of the solvent and reservoir oil system can be found through swelling calculations. The third column in Table 13 shows the saturation pressure calculated by swelling test for each of the solvent mixture and

reservoir fluid systems when the mole fraction of the solvent mixture is 0.85.

Examining the saturation pressure of the solvent mixture and of the solvent plus reservoir fluid, it is shown in Figure 6 that the dew point pressures of the solvent mixtures all fall below the saturation pressures of the solvent mixture plus reservoir fluid systems, except for No. 2, which represents the $0.3C_1+0.2C_2+0.5C_3$ combination. Because the original oil contained a significant amount of C_1 (original mole fraction of C_1 is 23.3%), when injecting C_2 into the reservoir, part of C_1 was displaced by C_2 and thus the pressure level was reduced for the solvent mixture plus oil. For this particular type of reservoir fluid, C_2 is not recommended as a solvent candidate.

The dew point pressure is not always proportional to the cumulative oil production. There exist optimal values in between. The cumulative oil production and the dissolved C_3 in the produced oil vs. the mole fraction of C_1 in the solvent mixture are plotted in Figures 7 and 8, respectively. The dissolved C_3 follows the same trend as the cumulative oil production. At a C_1 mole fraction of 0.39, the cumulative oil production reaches a maximum, as does the amount of C_3 dissolved in the produced oil.

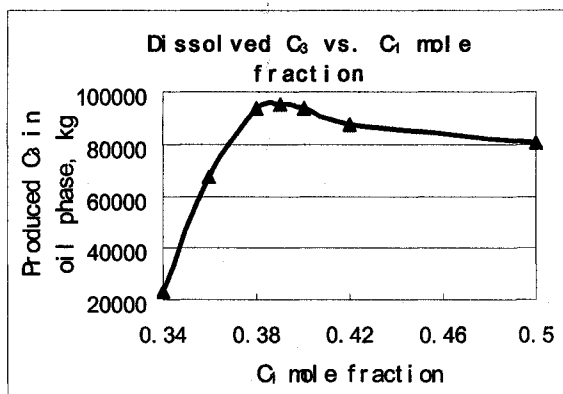


Figure 7. Dissolved C_3 vs. C_1 mole fraction

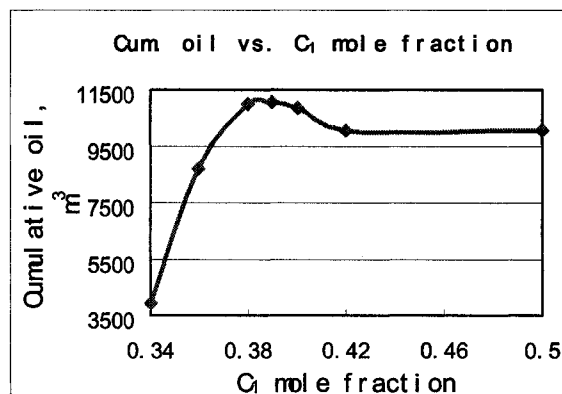


Figure 8. Cum. oil vs. C_1 mole fraction

The mole fractions of C_1 from 0.38 to 0.4 give similar results in cumulative oil production and dissolved C_3 in the produced oil. Thus, for our study, a solvent mixture of $0.39 C_1 + 0.61 C_3$ is taken as the optimal solvent.

4.5.3 Solvent Effect on Heavy Oil

Once the optimal solvent was found, the phase behavior of the solvent mixture and oil system were examined via a two-phase envelope calculation in WinProp. Two pseudo-ternary plots were generated under at 21°C for pressures of 5000 and 8000 kPa. These plots are shown in Figures 9 and 10, respectively.

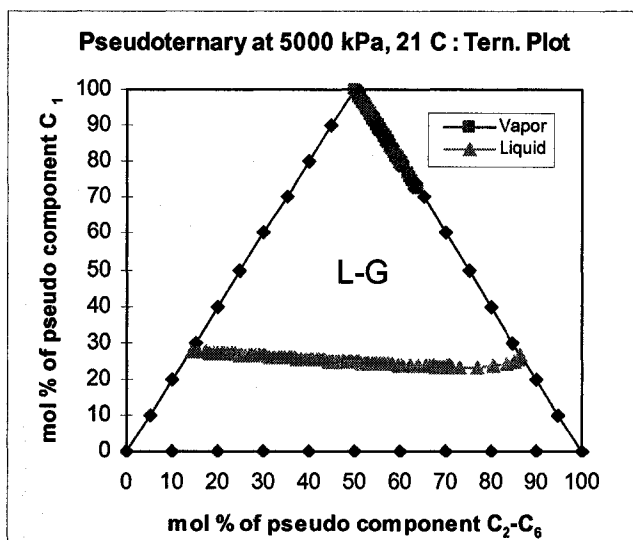


Figure 9. Ternary Plot at 5000 kPa, 21 °C

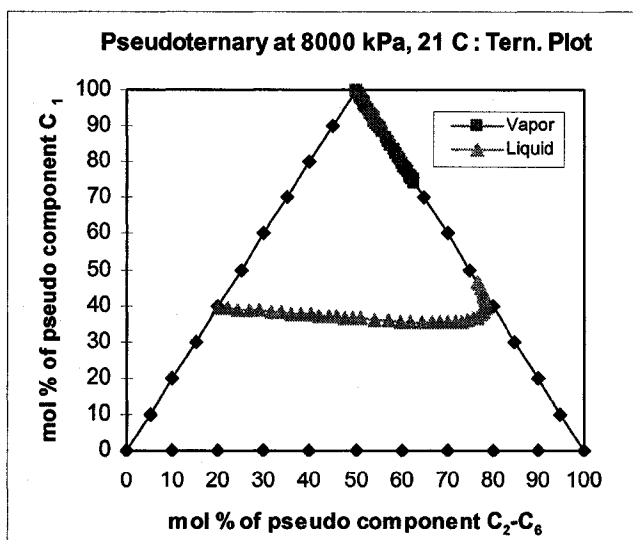


Figure 10. Ternary Plot at 8000 kPa, 21°C

The three corners in the ternary plot represent the light hydrocarbon components C₁ and

C_{1B} , the intermediate components C_2-C_6 , and the heavy end hydrocarbon components C_{7+} . A comparison of the two ternary plots shows that, at different pressures, the two-phase vapor and liquid (V and L) region is reduced when the pressure is increased from 5000 to 8000 kPa.

In addition, a swelling test and a two-phase flash for the same multiple component solvent and heavy oil system was also calculated. The results are shown in Figures 11 and 12, respectively.

In Figure 11, as the mole fraction of the solvent ($0.39C_1 + 0.61C_3$), increases from 0 to 0.85, the saturation pressure of the oil and solvent system increases at the same time. A bubble point pressure range of around 4000-8000 kPa is achieved with a maximum swelling factor of 2.0. After the concentration of the solvent reaches 0.6, the swelling factor increases considerably.

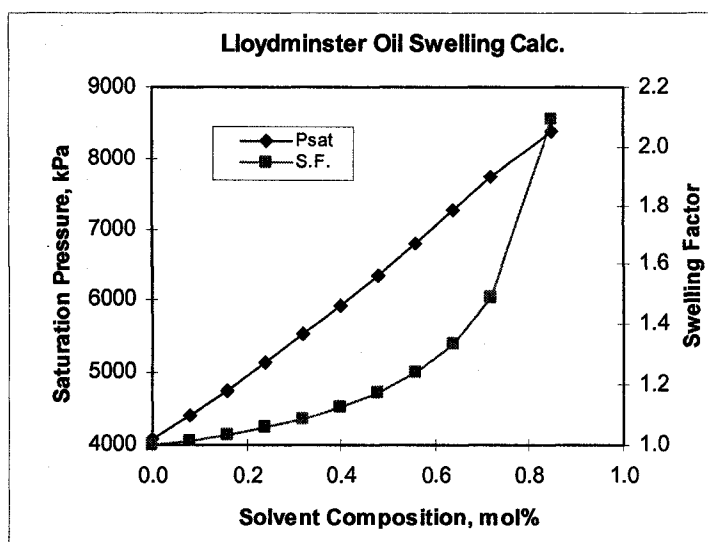


Figure 11. Swelling Test

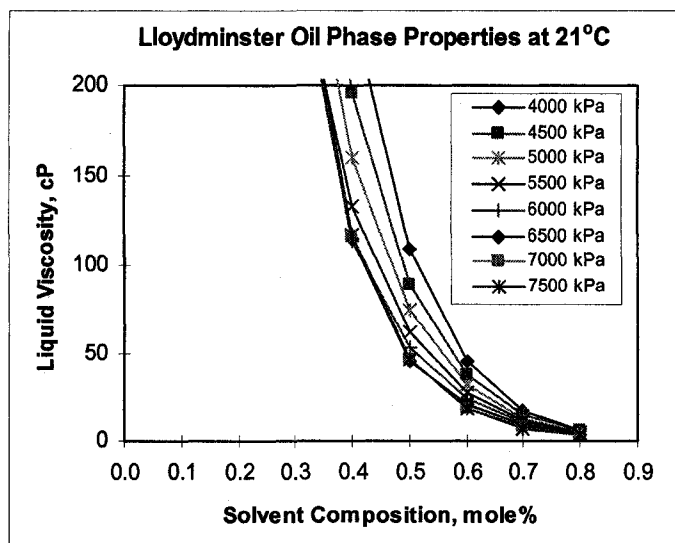


Figure 12. Two Phase Flash

Figure 12 shows the changes in the viscosity of the solvent mixture and oil system with varying concentrations of the solvent mixture at different pressure levels. Higher pressure gives lower viscosity at the same solvent concentration because more solvent is dissolved into the heavy oil at higher pressures. The changes become less obvious when the pressure is greater than 6000 kPa. On the other hand, only when the solvent concentration reaches 0.4 at pressures higher than 6000 kPa, does the heavy oil become mobile, resulting in a viscosity of less than approximately 100 cp.

4.6 Numerical Simulation

4.6.1 Reservoir Description

A typical Lloydminster-type reservoir was considered as a reference for designing the properties of the studied reservoir. Published data^{42,43}, such as reservoir depth and initial pressure, permeability and porosity data were used, and are shown in Table 14. End points values of the Lloydminster reservoir were used to generate the relative permeability curves. The temperature was set at 21°C: the whole process was isothermal. Rock compressibility is $7.4 \times 10^{-6} \text{ kPa}^{-1}$ at a reference pressure of 101.3 kPa.

Table 14. Reservoir Description

Porosity	33%
Permeability i_j	2 Darcy
Permeability k	1 Darcy
Reservoir top depth	450 m
Temperature	21 °C
Initial pressure at 450 m	4076 kPa
Initial oil saturation	0.75

The relative permeability curves were generated using the STONE 2 correlation and the end points were selected based on published results. Figures 13 and 14 show the relative permeability curves vs. water saturation and liquid saturation, respectively. Their corresponding data are listed in Tables 15 and 16.

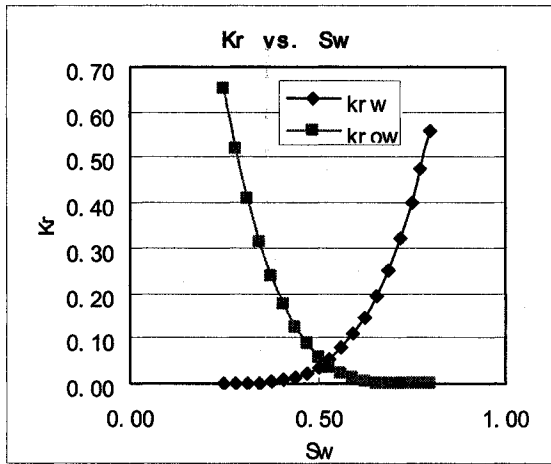


Figure 13. K_{rw} and K_{row} vs. S_w

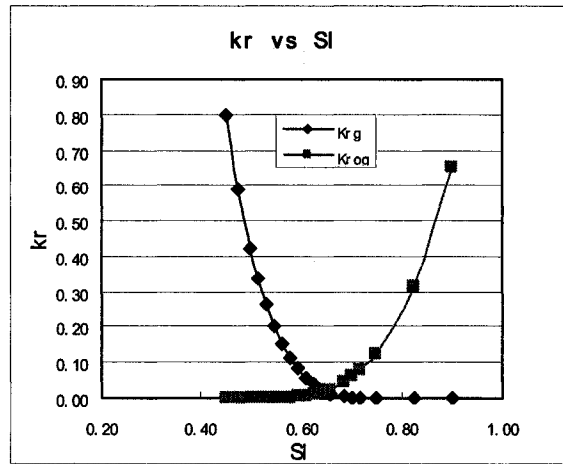


Figure 14. K_{rg} and K_{rog} vs. S_L

Table 15. K_{rw} and K_{row} vs. S_w

S_w	K_{rw}	K_{row}
0.25	0.00	0.65
0.28	0.00	0.52
0.31	0.00	0.41
0.34	0.00	0.31
0.38	0.00	0.24
0.41	0.01	0.18
0.44	0.01	0.13
0.47	0.02	0.09
0.50	0.04	0.06
0.53	0.05	0.04
0.56	0.08	0.02
0.59	0.11	0.01
0.63	0.15	0.01
0.66	0.19	0.00
0.69	0.25	0.00
0.72	0.32	0.00
0.75	0.40	0.00
0.78	0.48	0.00
0.80	0.56	0.00

Table 16. K_{rg} and K_{rog} vs. S_L

S_L	K_{rg}	K_{rog}
0.45	0.80	0.00
0.48	0.59	0.00
0.50	0.42	0.00
0.52	0.34	0.00
0.53	0.26	0.00
0.55	0.20	0.00
0.56	0.15	0.00
0.58	0.11	0.00
0.59	0.08	0.00
0.61	0.06	0.01
0.63	0.04	0.01
0.64	0.02	0.02
0.66	0.01	0.02
0.69	0.0033	0.05
0.70	0.0012	0.06
0.72	0.0003	0.08
0.75	0.0000	0.13
0.825	0.0000	0.31
0.9	0.0000	0.65

4.6.2. 2D simulation settings

The simulation setting parameters are listed in Table 17. The grid type was selected as Cartesian, and the grid block system was $120 \times 1 \times 20$, giving 2400 grid blocks in total. In GEM, for each grid block, the simulator performs the flash calculation first for each single component at each grid block and at each time step. The size of the grid block needs to be very small; the smaller it is, the more accurate the calculations will be. However limited by the academic version of the simulator used at the University, the grid block size was selected as $1\text{m} \times 1\text{m}$ for both the i and k directions. For the j direction, there was only one grid block, and the length of the horizontal well was exactly the length of the j direction, 600 meters.

The reservoir size can be calculated according to the grid block system settings:

$$\text{-Volume of the reservoir} = 120 \times 600 \times 20 = 1,440,000 \text{ m}^3$$

$$\text{-OOIP} = 144,0000 \times \Phi \times S_{oi} / B_{oi} = 144,0000 \times 33\% \times 0.75 / 1.033 = 345,015 \text{ m}^3$$

Table 17. 2D simulation settings

Grid type	Cartesian
Grid block system (i,j,k)	120 x 1 x 20
Grid dimension (i,j,k)	1m x 600m x 1m
Number of pseudo-Components	8
EOS	PR -1979
Solvent composition	39%C1 + 61%C3
Number of horizontal injectors	2, at layer 12
Number of horizontal producers	2, at layer 17
Constant injection rate	4500 m ³ /day
Minimum BHP at producer	4100 kPa

Two horizontal well pairs were used for developing the entire reservoir. The horizontal injection well was placed above the horizontal production well. The vertical distance between the injector and the producer was five meters, and the horizontal distance between the two well pairs was 80 meters, as shown in Figure 15.

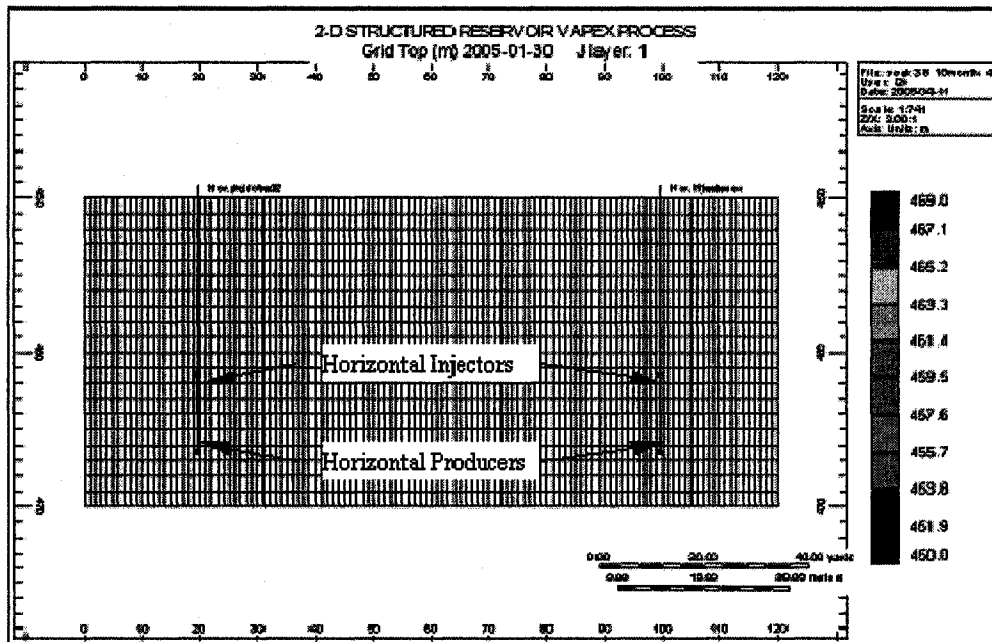


Figure 15. Front View of the simulation settings

4.6.3 Initial Conditions

There is initially no gas cap within the reservoir; water and oil were the only phases present. Block saturation at each grid block is averaged over the depth interval spanned by the grid block, gravity and capillary equilibrium are calculated. A phase pressure correction is added to ensure that the reservoir is initially at gravitational equilibrium. The initial pressure is 4076 kPa at the top of the reservoir, 450 meters in depth, and the water-oil contact depth is located at 470 meters.

CHAPTER 5

ANALYSIS OF SIMULATION RESULTS

5.1 Optimal Soaking Time

The concept of cyclic solvent injection is very similar to cyclic steam injection^{44,45}. Following each injection period, the production wells are shut in and the soaking period starts. During this phase, the solvent will move further away from the injection well and take effect with the heavy oil, diluting it in the porous medium. The optimal soaking time will result in the most effective viscosity reduction and the lowest GOR.

Different injection times will result in different optimal soaking times. Considering that cyclic solvent injection performance follows the fact that the subsequent cycle requires more solvent than does the previous one, where some of the reservoir oil around the well bore and nearby locations is produced. Three-month, 6-month and 9-month injection cases have been considered and their respective optimal soaking times were determined.

5.1.1 Three-month injection case

For the 3-month injection case, the viscosity reduction profiles at one of the production wells were compared for the no soaking, 3-month, 4-month, and 5-month soaking times. The results are shown in Figure 16. In this figure, time zero indicates the start of injection. The critical soaking time for a given injection cycle is defined as the time at which the viscosity of the oil is reduced to less than 100 cp during the production phase.

For the case where no soaking took place, the viscosity did not reach the requirement of 100 cp until eight months into the production phase. It then increased as production proceeded. It can be seen that, during the longer soaking times, lower viscosities were obtained in the long term. The viscosity curve for the 4-month and 5-month soaking times were very close to each other. Considering time constraints, it is not necessary to soak for one additional month. Thus,

the optimal soaking time, for a 3-month solvent injection, was determined to be the 4-month soaking time.

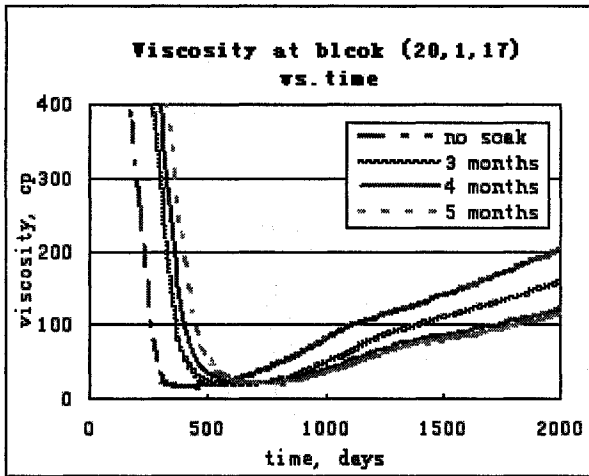


Figure 16. Viscosity Profile – 3-month Inj.

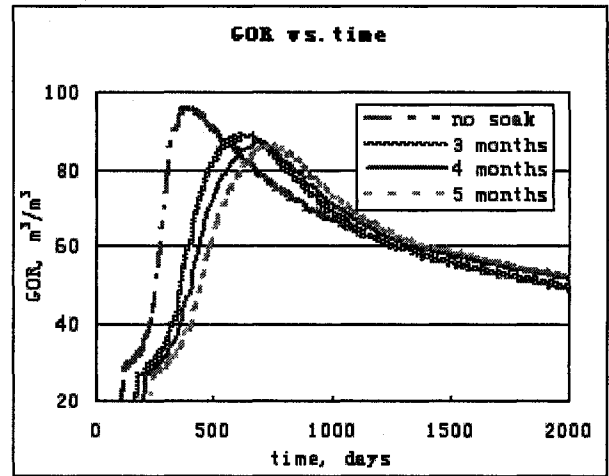


Figure 17. GOR Profile – 3-month Inj.

This result can be ascertained by analyzing the GOR profile in Figure 17. The GOR increases quickly during the early stages of production, and declines after reaching a peak value. The no soaking case gave the highest peak GOR value, which means that more of the injected gas was produced rather than dissolved in the oil, as compared with the other three cases. The longer soaking times gave the lowest peak GOR values. The results for the 4-month and 5-month soaking times were very close to each other. We therefore selected the 4-month soaking time as the optimal value.

Moreover, it is worth mentioning that the heavy oil viscosity reduction occurs instantaneously if the concentration of the solvent is large enough at the production well. This phenomenon has been observed in previous work⁹. The amount of solvent required for this depends on the time it takes for the solvent to be transported over the 5 m distance separating the injection well from the production well.

5.1.2 Six-month injection case

Similarly, for the 6-month solvent injection case, Figure 18 shows the viscosity profile over time. It looks similar to the 3-month injection case, with a disturbance (spike) in the middle

section of the figure. This may be caused by asphaltenes precipitation, but needs to be investigated further. As more solvent was injected into the reservoir in this case, the time at which the 100 cp level was achieved was about two months earlier than in the 3-month injection case.

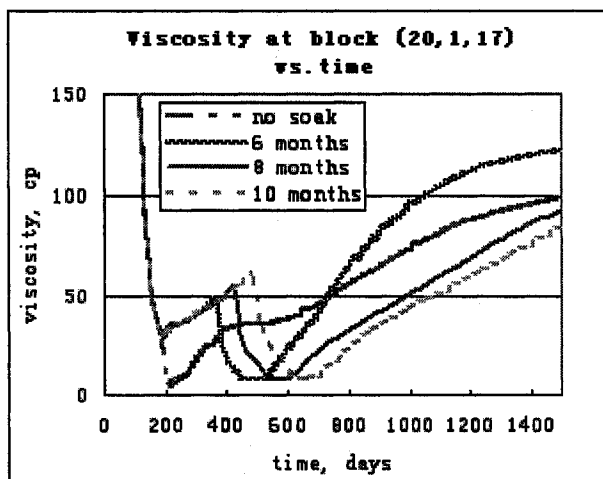


Figure 18. Viscosity Profile – 6 month Inj.

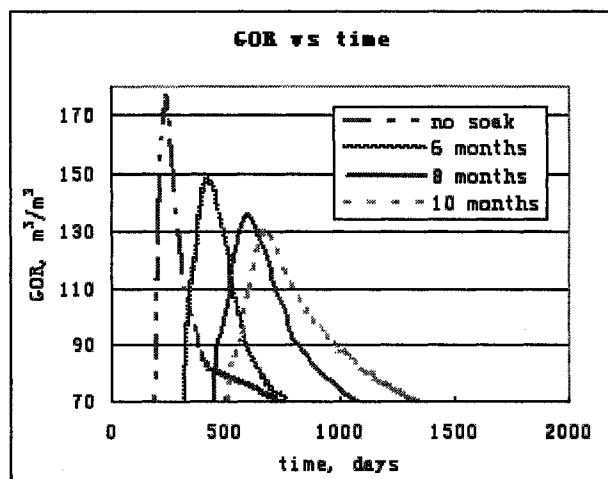


Figure 19. GOR Profile - 6 month Inj.

An 8-month soaking time resulted in a lower long-term viscosity, as compared with the 6-month soaking time, and a similar long-term viscosity to the 10-month soaking time. Also, the GOR profile shown in Figure 19 indicates that an 8-month soaking time is better than a 6-month soaking time and that it is very similar to a 10-month soaking time. Therefore, an 8-month soaking time was determined to be the optimal soaking time for the 6-month solvent injection case.

The cumulative production rate can be used as another way to determine the optimal soaking time. In Figure 20, the cumulative oil productions at the end of 10 years of operation (injection-soak-production) are compared to illustrate how much oil can be produced for different soaking times. The longer the soaking period is, the higher the cumulative oil production is.

The no soaking and 6-month soaking cases, which resulted in the lowest cumulative amounts of production, had similar amounts of cumulative production. The 8-month soaking case enhanced the cumulative production by 10% percent compared with the no-soaking and 6-month soaking cases. The difference between the 6- and 8-month soaking times was greater than the

difference between the 8- and 10-month soaking cases. This is another confirmation that the 8-month soaking time is the optimal soaking time for the 6-month solvent injection case.

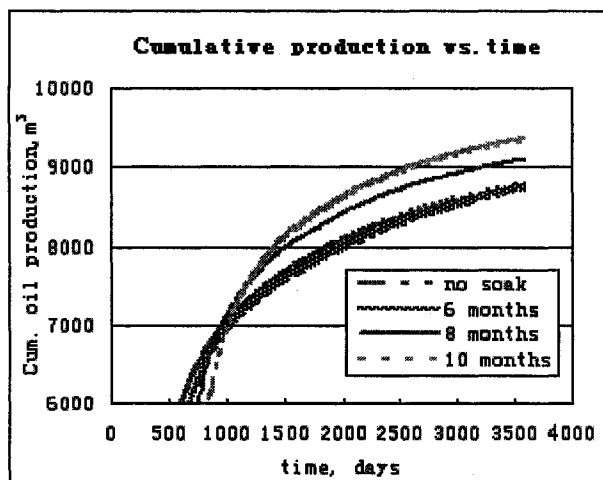


Figure 20. Cumulative Prod. – 6 month Inj.

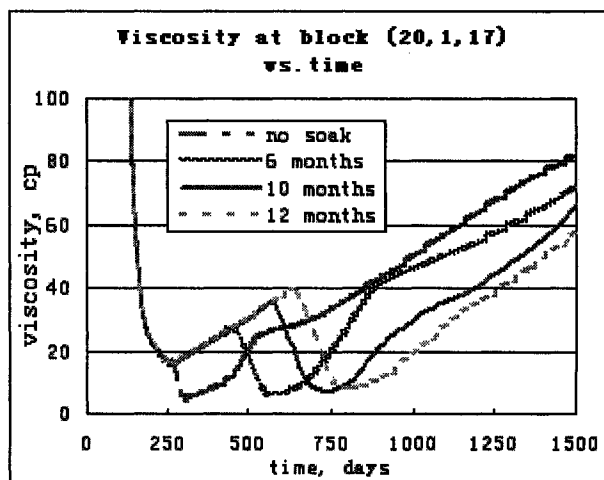


Figure 21. Viscosity Profile - 9 month Inj.

5.1.3 Nine-month injection case

In the 6- and 9-month solvent injection cases, the viscosity profiles exhibit similar behavior, as can be seen from Figures 18 and 21. The viscosity spike is more pronounced than in the previous case, where the soaking time was longer. It might have been easier for the asphaltenes to precipitate, because this phenomenon only occurs⁹ when the solvent reaches a high enough concentration at reservoir conditions.

The 10-month soaking time gave a better overall solvent performance in this case. The GOR profile in Figure 22 supports the same conclusion as the viscosity profile. In addition, by examining the cumulative oil production profiles (Figure 23), it can be inferred that the 10-month soaking time was the optimal soaking time for the 9-month solvent injection case.

In conclusion, the optimal soaking times for the 3-, 6-, and 9-month solvent injection cases were found to be 4, 8, and 10 months, respectively.

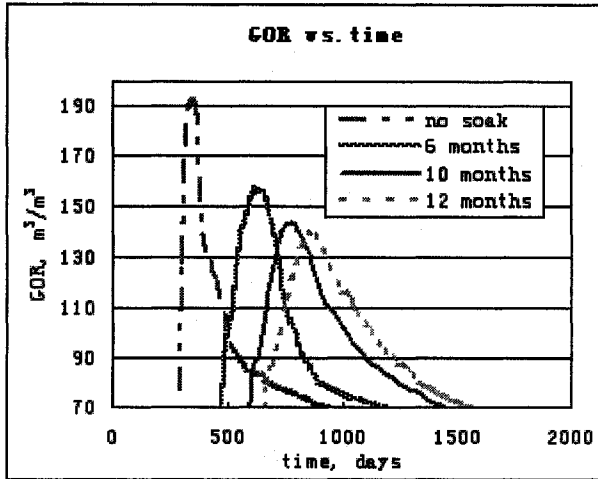


Figure 22. GOR profile – 9 month Inj.

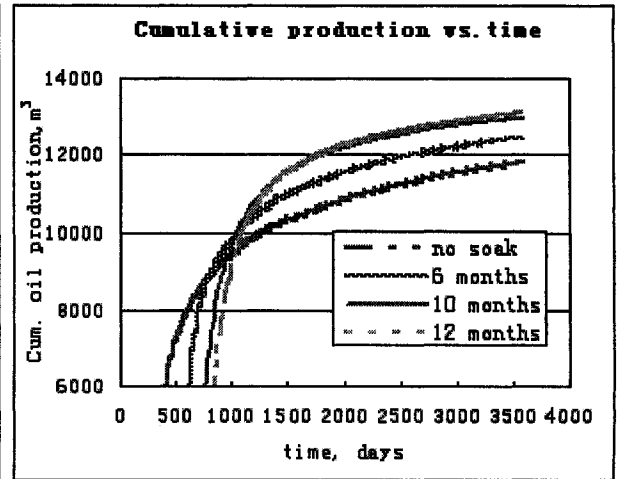


Figure 23. Cum. Prod. – 9 month Inj.

5.2 Cycles Design

The main principles of the cyclic steam injection strategy^{40,41} were applied to the cyclic solvent injection. Accordingly, the injection, soaking, and production periods for each cycle have to be designed properly in order to maximize the oil production. The production time following each cycle can also be determined by analyzing the production decline curves.

Different combinations of injection times were run numerically and compared to optimize the cycle's design based on the optimal soaking times, determined in the previous chapter. The following sequences were considered:

3-month injection --- 4-month soaking --- 12-month production

6-month injection --- 8-month soaking --- 24-month production

9-month injection --- 10-month soaking --- 36-month production

Another reason for the cycle's design is to try to discern which one is better: short, intermediate, or long injection cycles? Combinations of the 3-month, 6-month, and 9-month cycles were run according to the trial and error method. The various cycles shown in Table 18 were simulated. The NCSOR values were calculated for each case, and are compared in the following section.

Table 18. Cycles Design

No.	Cycles	Injection time	Soaking time	Production time
1	3, 3, 3	3, 3, 3	4, 4, 4	12, 12, 12
2	3, 3, 6	3, 3, 6	4, 4, 8	12, 12, 24
3	3, 6, 6	3, 6, 6	4, 8, 8	12, 24, 24
4	6, 6, 6	6, 6, 6	8, 8, 8	24, 24, 24
5	3, 6, 9	3, 6, 9	4, 8, 10	12, 24, 36
6	no soak	3, 3, 6	0, 0, 0	12, 12, 24

Note: in the above table, time is measured in month

5.3 NCSOR

Since very little field data is available for the VAPEX process, it is hard to accurately evaluate its economic performance. The value of NCSOR, which represents the net cumulative ratio of the injected solvent to the produced oil, thus becomes an effective economic indicator for the solvent-based heavy oil recovery process; it is very similar to SOR, the steam-oil ratio, in the SAGD process.

The cumulative solvent consumed is calculated by deducting the solvent produced from the solvent injected for each case. The NCSOR value is obtained, with units of kg/kg, by dividing the above quantity by the cumulative oil produced. This calculation is conducted with the assumption that no solvent leakage or loss occurred during the process. The material balance for the solvent is as follows:

$$\text{Solvent injected} = \text{Solvent produced} + \text{Solvent left behind in the reservoir}$$

The solvent could be either in the gaseous or the liquid phase.

The quantities of C_1 and C_3 are analyzed in the compositional analysis section, where explanations of C_1 and C_3 consumption are provided in detail.

The results were obtained under the condition that the shut-off oil production rate was 5 m³/day for all the cycles. This shut-off rate could vary case by case; here 5 m³/day was assumed

to be the economic limit. So, when the instantaneous oil rate fell below this limit production was stopped, and a new cycle started.

Table 19. NCSOR Comparison

No.	Cycles month	NCSOR 5 m ³ /day
2	3, 3, 6	0.11
4	6, 6, 6	0.12
3	3, 6, 6	0.13
5	3, 6, 9	0.13
1	3, 3, 3	0.15
6	no soak	0.16

As shown in Table 19, run No. 2, representing a three-cycle case, with a 3-month injection period followed by its optimal soaking and production periods, another 3-month injection with associated optimal soaking and production, and finally a 6-month injection, soaking, and production, attains the most attractive NCSOR value of 0.11. Runs No. 4, 3, and 5 yielded similar results, however run No.1 gave worse results. This is because, in the first cycle, there was not enough solvent in the 3-month injection period to dilute the heavy oil between the injector and producer; thus, not much oil could be produced during the first cycle. After this, the amount of solvent should be increased in order to produce more oil.

For the no-soaking case, the cycles were the same as in the best case, run No. 2. The only difference is that, after injection, the production period followed directly without any soaking. The no soaking case yielded the worst NCSOR result and the difference between this case and the soaking case was about 0.05.

5.4 Comparison of Soaking and No soaking cases

5.4.1 Simulation Results Comparison

The main difference between soaking and no soaking is the soaking period following the injection period. For the no soaking case, the production period will start right after the injection period. Thus, for the no soaking case, production will occur earlier than it will for the soaking case; however, due to the shorter interaction time between the solvent and the heavy oil, production will decline faster. For the soaking case, production will happen later, but since the solvent moves further away from the injection well and contacts the heavy oil to dilute it more, the oil will become mobile and will be produced more easily.

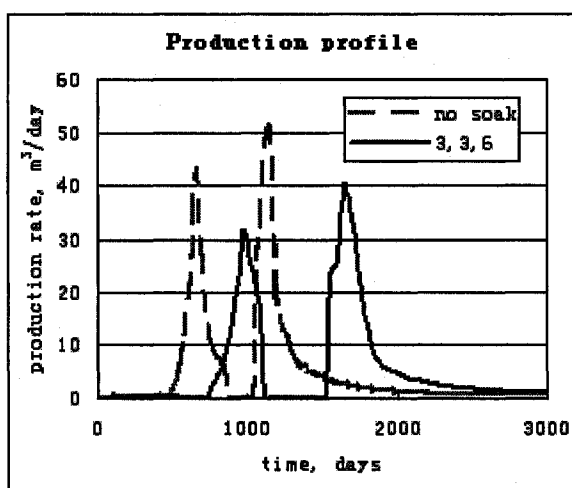


Figure 24. Production Comparison

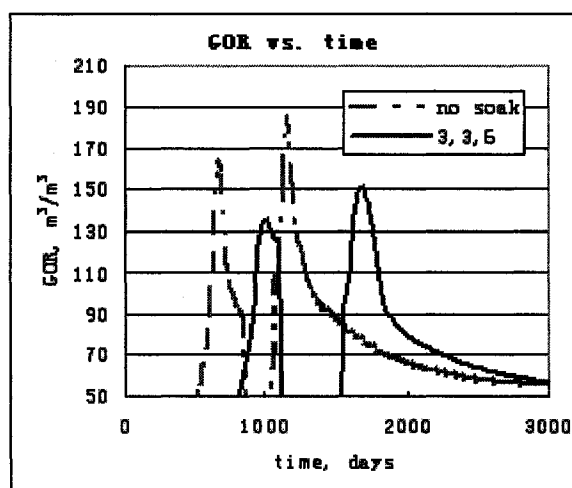


Figure 25. GOR Comparison

There are three cycles for both the soaking and the no soaking cases, however, due to the small amount of solvent injected in the first cycle, the production is not visible. The following cycle works because during the first cycle, some of the solvent interacts with the heavy oil and reduces its viscosity. It is therefore easier to produce the heavy oil which has solvent dissolved in it.

The peak production rate in the no soaking case is around 10 m³/day higher than the soaking case, as is shown in Figure 24. This is because, when there is no soaking, the injected gas accumulates mainly around the injection well so that the pressure difference between the horizontal injector and the producer is larger than in the soaking case, where the gas has already

been transported further away from the injection well. In the soaking case, a wider vapor chamber has been created.

On the other hand, the area under the production curve is smaller in the no soaking case than in the soaking case where more mobile heavy oil has been generated during the soaking period. The production curve is similar to that of a solution gas drive.

Figure 25 displays the GOR performance of the soaking and no soaking cases. The GOR curves are similar in shape to the production curves. There is a maximum GOR value difference of approximately $20 \text{ m}^3/\text{m}^3$ between the no soaking and soaking cases. This is reasonable because, for the no soaking case, the solvent is injected into the reservoir and the production cycle begins right after the injection cycle. Consequently, most of the solvent will be produced instead of moving further up or sideways inside the reservoir.

The cumulative production of the soaking and no soaking cases are also compared in Figure 26. The last two cycles contribute mainly to the cumulative production. The no soaking case is ahead during the first part of the production life. However, after 2000 days, the soaking case overtakes it and ends with around 10% higher cumulative production. The soaking case produces more cumulative oil, but when time is taken into consideration, the no soaking case produces the oil earlier. The optimal case would depend on the cost of solvent, the price of oil, as well as on many other economic considerations.

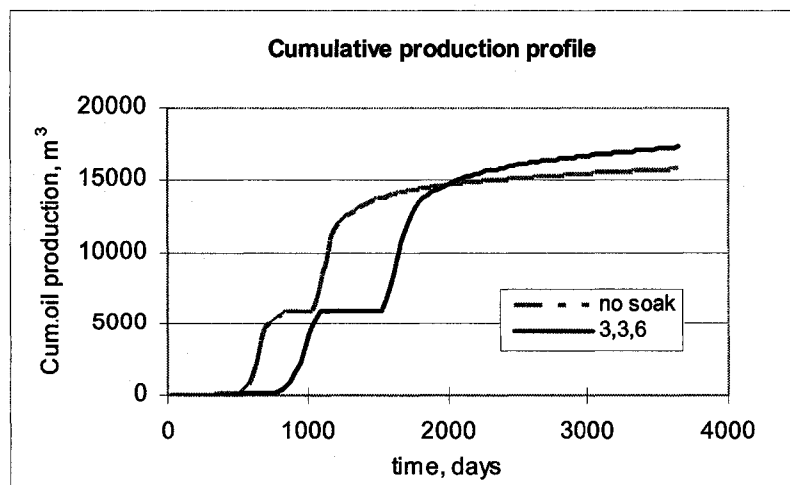


Figure 26. Cumulative Production

5.4.2 What happens during the soaking period?

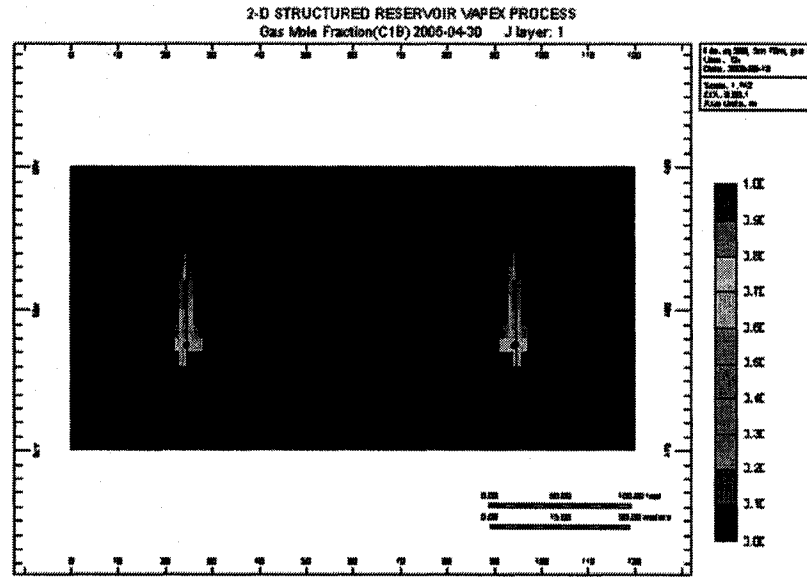


Figure 27. Gas mole fraction (C_{1B}) at 2005-04-30, No-soaking

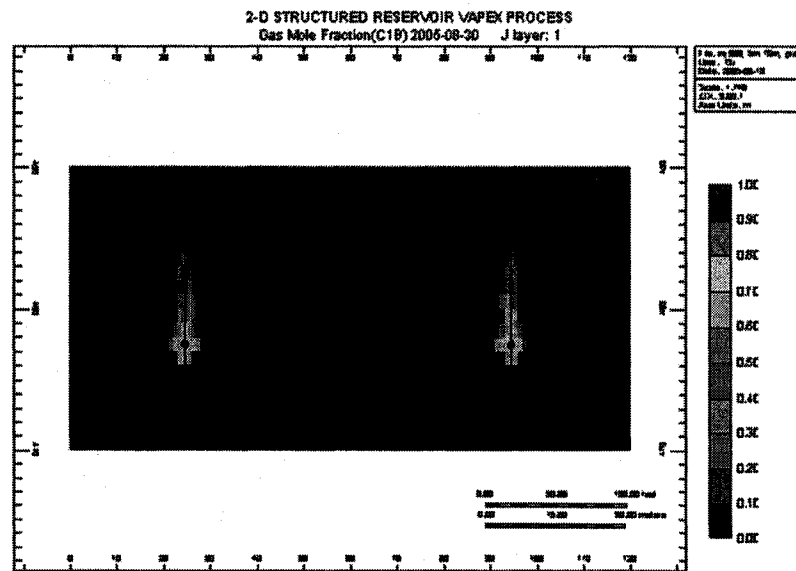


Figure 28. Gas mole fraction (C_{1B}) at 2005-08-30, Soaking

The gas mole fractions of C_{1B} and C_3 , and the oil mole fractions of C_{1B} and C_3 at the beginning of each production cycle are compared for the soaking and no soaking 3,3,6 cycles. Table 20 gives the start date of each production cycle for both the soaking and no soaking cases. Since the soaking case needs two periods of 4-month soaking and one of 8-month soaking, there

is a 16-month total delay compared to the no soaking case. Both the soaking and no soaking cases have the same amount of solvent in the reservoir for the first cycle.

Table 20. Schedule of the Production Cycles

Cycle no.	start time of production cycle	
	no soaking	soaking
1	2005- 4- 30	2005- 8- 30
2	2006- 5- 30	2007- 1- 30
3	2007- 11- 30	2009- 3- 30

First production cycle - gas mole fraction of C_{1B} :

Figures 27 and 28 show the mole fractions of C_{1B} for the no soaking and soaking cases, respectively. Both of them are recorded at the beginning of the first production cycle. Different colors, from blue to red, represent different mole fractions, changing from 0 to 1. Since the two well pairs have the same operating conditions, the two vapor chambers have almost identically developing shapes. There may be slight differences between the two shapes due to the non-linearity of the problem. It is easier to compare the soaking effect if one considers only one of the vapor chambers from Figures 27 and 28 and puts them together in Figure 29.

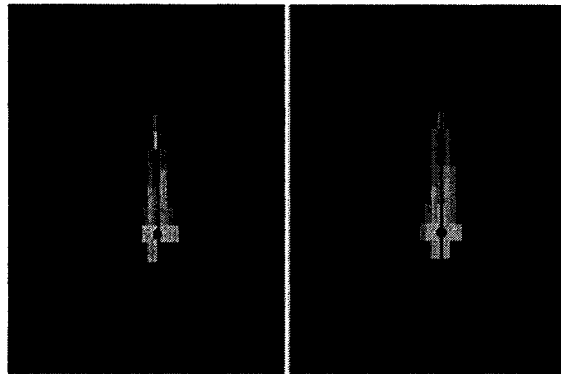


Figure 29. Gas mole fraction of C_{1B} , 1st Cycle

The image on the left represents the no soaking case, and the one on the right is the soaking case. The mole fraction of C_{1B} for the soaking case was greater than that of the no soaking case, and the most C_{1B} , represented by the red colored line, moved to the upper part of the reservoir during the soaking time. The resulting C_{1B} distribution is due to the soaking effect.

This also explains why the peak production rate for the no soaking case was higher than that of the soaking case. In the no soaking case, most of the methane accumulated above the injector and, as a consequence, the pressure around the injector was higher than the pressure at the same grid block in the soaking case. Thus, more of the oil was pushed to the producer. It works the same way for GOR. During the soaking period, more of the methane gas moved to the upper part of the reservoir and less was produced. As for the cumulative production in the soaking case, more oil was displaced because more oil in the upper part of the reservoir got the chance to contact the solvent.

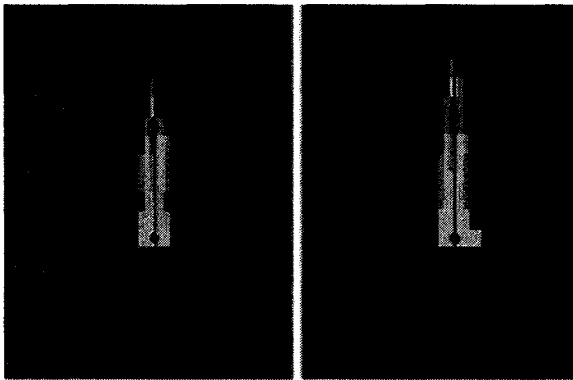


Figure 30. Gas Mole fraction of C_{1B} , 2nd Cycle

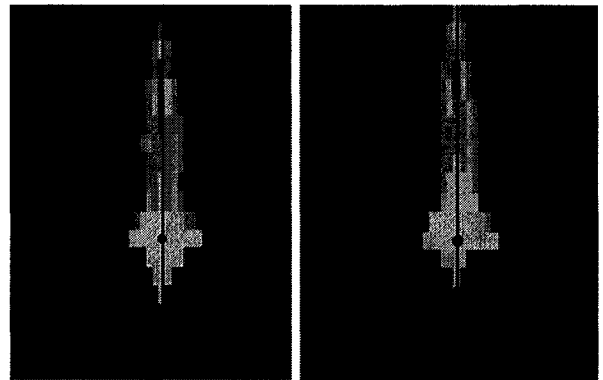


Figure 31. Gas Mole fraction of C_{1B} , 3rd Cycle

Second and third production cycles:

The size of the vapor chamber became larger and larger for the 2nd and 3rd cycles as shown in Figures 30 and 31. As in Figure 29 (1st cycle), the images on the left represent the no soaking case, and the ones on the right the soaking case. Most of the methane accumulated at the top of the reservoir and, for the soaking case, the methane was distributed at a higher level in the reservoir than in the no soaking case.

Gas mole fraction of C₃:

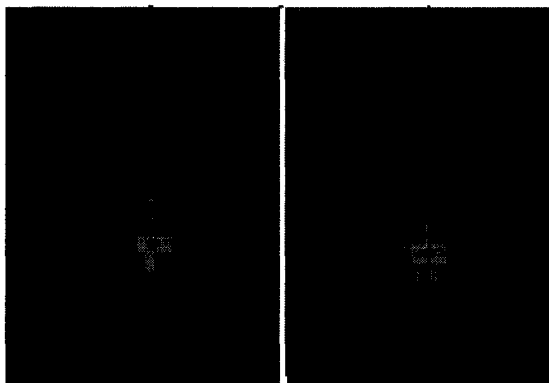


Figure 32. Gas mole fraction of C₃, 1st Cycle

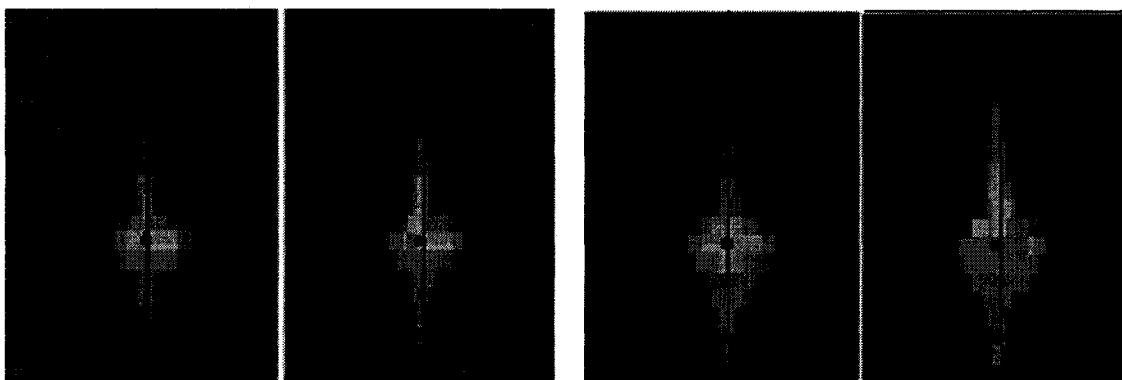


Figure 33. Gas Mole fraction of C₃, 2nd Cycle Figure 34. Gas Mole fraction of C₃, 3rd Cycle

Propane has the same vapor-chamber developing trend as methane. As can be seen in Figures 32, 33, and 34, the size of the chamber for the no soaking case was always smaller than the size of the vapor chamber for the soaking case. More gas was produced in the no soaking case right after the injection period, however, for the soaking case, the gas moved to the other part of the reservoir so the shape was more dispersed.

The color of these Figures, as compared to C_{1B}, indicates that the amount of gaseous C₃ was much less, although the injected solvent mixture contained 0.39 C_{1B} and 0.61 C₃. The major colors for the C₃ chamber were green and yellow; for C_{1B} there was also red, which represents 100% saturation of the gas considered. This is because the dew point pressure of C₃

is much less than that of C_{1B} ; the liquefied C_3 dissolved into the oil phase.

The following figures will show the mole fraction of C_{1B} and C_3 in the oil phase.

Oil mole fraction of C_{1B} :

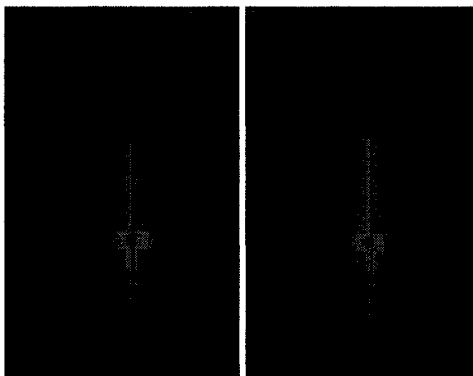


Figure 35. Oil mole fraction of C_{1B} 1st Cycle

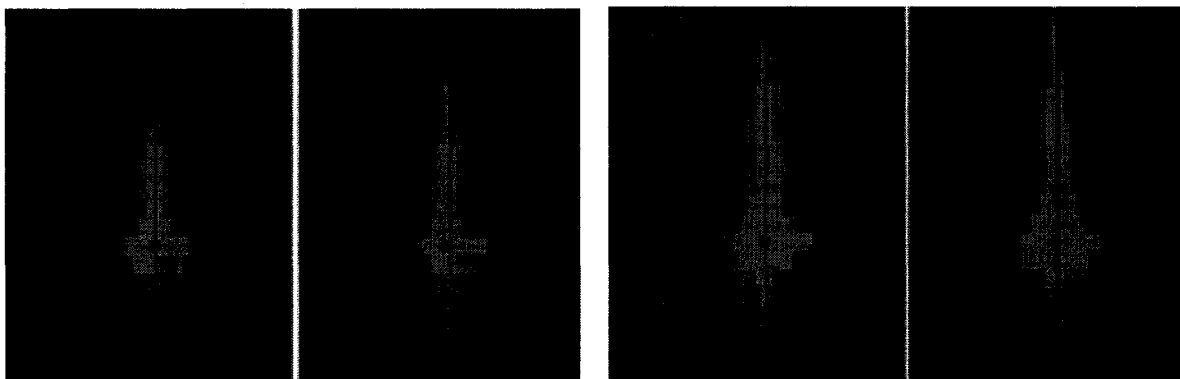


Figure 36. Oil Mole fraction of C_{1B} , 2nd Cycle

Figure 37. Oil Mole fraction of C_{1B} , 3rd Cycle

From the above Figures 35 through 37, it is apparent that the development of the solvent chamber of dissolved methane in the no soaking case for the first and second cycles was slower than in the soaking case. Thus, soaking helps promote the solvent dissolution into the oil phase. As for the third cycle, the reservoir oil was saturated with methane, and the shapes for the soaking and no soaking cases are very similar.

The concentrations of C_{1B} in the chamber for all three cycles were quite similar, which is symbolized by the same light blue color representing 0.2-0.3 mole fractions. This means that the reservoir oil was saturated with methane at about this concentration; it can not dissolve more

methane than this. The development of propane dissolved in the oil phase has different results.

Oil mole fraction of C₃:

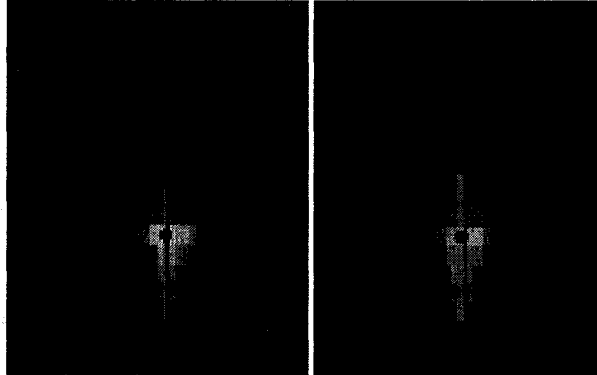


Figure 38. Oil mole fraction of C₃, 1st Cycle

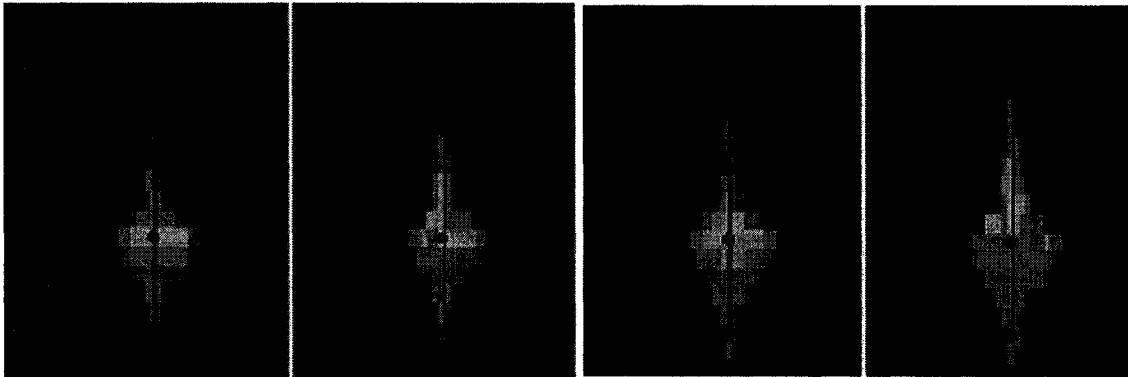


Figure 39. Oil mole fraction of C₃, 2nd Cycle Figure 40. Oil mole fraction of C₃, 3rd Cycle

For the first cycle shown in Figure 38, the soaking and no soaking cases have the same amount of injected propane. However, in the no soaking case, more propane accumulated around the injection well, as is indicated by the orange color, surrounding the injector. In the soaking case, the propane is more evenly distributed around the injector, due to the soaking effect. Thus, oil that is further away from the injection well gets a chance to contact the solvent. The sweeping efficiency for the soaking case is higher than for the no soaking case.

Similar results were obtained for the second and third cycles shown in Figures 39 and 40. The size of the oil phase C₃ is always larger in the soaking case, and C₃ is distributed more evenly. This also further illustrates why the cumulative production of the soaking case is always higher

than that of the no soaking case when the same amount of solvent is injected into the reservoir.

Comparing the oil phases C_{1B} and C_3 , the shape of the C_{1B} in Figures 35 through 37, is much narrower. The shape of C_3 in Figures 38 through 40, is wider. In the reservoir, due to the different dew point pressures of methane and propane, the methane is predominantly gaseous. Therefore, it moves up into the reservoir. Propane, on the other hand, is in the liquid phase and moves all around. However, it tends towards a downward movement because of gravity.

5.4.3 Solvent Left Behind

The solvent left behind in the reservoir was calculated for the three cycles, 3,3,6, for the soaking and no soaking cases. Results showed that, for the soaking case, around 61% C_1 was left behind in the reservoir and for the no soaking case, 60% C_1 was left behind. As for C_3 , for the soaking case, there was around 35% C_3 left behind, and 34% C_3 was left behind in the reservoir for the no soaking case. The amount of solvent that was left behind in the reservoir for the soaking case is higher than that of the no soaking case, because of the movement of the solvent during the soaking period.

There are three possible phase types for the solvent left behind in the reservoir: it could be dissolved in the reservoir oil, as a free gas phase, or as a free liquid phase. Different cycles' designs will produce different values for the solvent left behind and longer soaking cases will have less solvent left behind.

5.5 Compositional Analysis

In situ upgrading is another potential advantage of the solvent-based heavy oil recovery process. It can help reduce the problems incurred during transportation and upgrading after the oil has been produced. In addition, the quality of the produced oil is better, and thus the price of the upgraded oil is higher.

At the end of the simulation work, a compositional analysis was performed to see the change in composition of the produced oil from the original oil. In Table 21, C_1 and C_{1B} are

combined into one component. The mole fraction changes for methane and the intermediate pseudo-components IC_4-NC_6 are quite small, less than 1%. The mole fraction of propane changed from 0.011% to 9.45%. The produced oil contains much more propane. The most important criterion for judging the upgrading aspect of the produced heavy oil is a comparison of the variation in these heavy end components. The mole fraction of the heaviest pseudo-component C_{33+} has been reduced by 4.14%, and the next heavy end pseudo-component, $C_{24}-C_{32}$, has been reduced by 1.92%. Both of these numbers indicate that the produced heavy oil has been upgraded after this solvent-based heavy oil recovery process.

Table 21. Compositional Analysis

No	Component	Dead oil (mole fraction)	Produced oil (mole fraction)	Change
1	C_1+C_{1B}	0.00%	0.26%	0.26%
2	C_2	0.00%	0.00%	0.00%
3	C_3	0.011%	9.45%	9.44%
4	IC_4-NC_6	0.431%	0.26%	-0.17%
5	C_7-C_{23}	37.09%	33.5%	-3.59%
6	$C_{24}-C_{32}$	19.62%	17.7%	-1.92%
7	C_{33+}	42.84%	38.7%	-4.14%

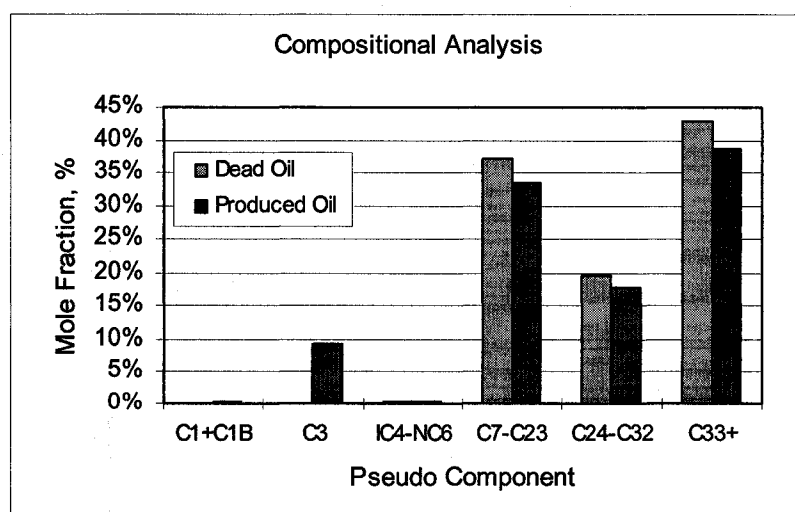


Figure 41. Compositional Analysis

Figure 41 compares the difference in composition between the dead oil and oil being produced after solvent injection. The change in propane composition is significant, and the changes in the composition of the other three pseudo-components, C_7-C_{23} , $C_{24}-C_{32}$, C_{33+} , are noticeable.

5.6 Well Configurations

In the cyclic solvent injection process, well configuration is another important design parameter. If the wells are configured properly, it can help enhance the oil recovery significantly. There are two well configuration parameters being considered: the vertical distance between the horizontal injection and the production wells, and the horizontal distance between the two well pairs, as shown in Figure 42.

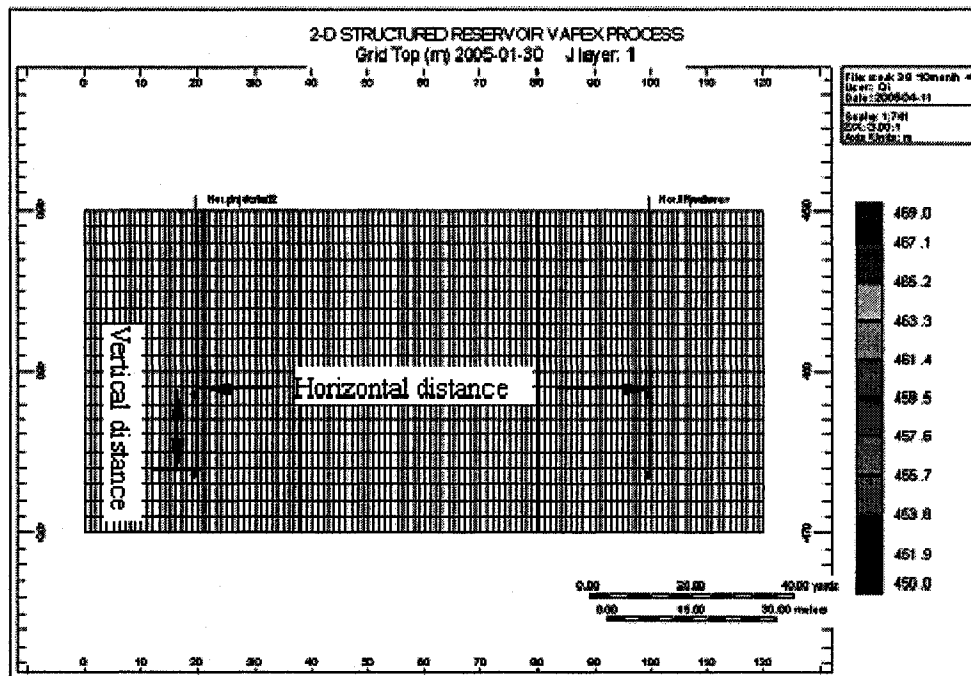


Figure 42. Front View of Well Configuration Parameters

Sensitivity analyses were performed for cycles 3,3,6, which represent 3-month injection, 4-month soaking, and 1-year production, another instance of the same cycle, followed by 6-month injection, 8-month soaking, and 2-year production, and 3,3,6,6,6, which represent the same

operational strategy as 3,3,6, but with the addition of two 6-month injection cycles and associated soaking and production periods. The purpose of this comparison was to examine whether the influence of well configuration varied with the amount of solvent injection or not.

For cycles 3,3,6, the vertical distance was fixed at five meters. Different horizontal distances ranging from 50 to 80 m, with 10 m as a step, were tested. The results are shown in Table 22 and Figure 43.

Table 22. Sensitivity Analysis of Horizontal Distance (3,3,6)

Horizontal	50 m	60 m	70 m	80 m
Cumulative production m ³	17158	17202	17332	16980
Difference m ³	178	222	352	0

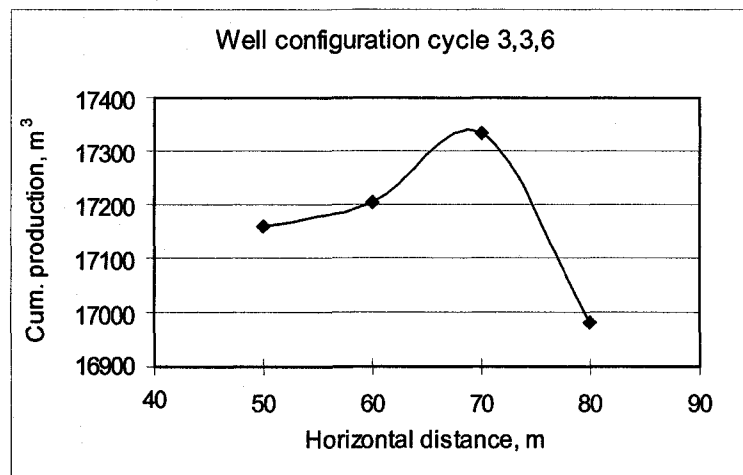


Figure 43. Sensitivity Analysis of Horizontal Distance (3,3,6)

The optimal horizontal distance is 70 m for this case, as indicated by the results from the comparison of cumulative production. The 80 m case is the worst scenario illustrated in Figure 43. The results of 50, 60, and 70 m are very close; there is around 100 m³ difference in oil production between them. If the two well pairs are too close, there is interference between the two injection wells. On the other hand, the solvent injected from one injection well helps reduce

the viscosity of the heavy oil, which is located between the two well pairs. If the distance is too great, the solvent injected from one injection well will not have any influence on the other well pairs.

Table 23. Sensitivity Analysis of Vertical Distance (3,3,6)

Vertical	5 m	6 m	7 m	8 m
Cumulative production, m ³	17332	18615	18780	9131
Difference, m ³	8201	9484	9649	0

The influence of the vertical distance on cumulative production is greater than that of the horizontal distance between the two well pairs. The cumulative production results in Table 23 were obtained based on a horizontal distance of 70 m, the optimal horizontal distance. A vertical distance of seven meters achieved the best results. These results are also plotted in Figure 44.

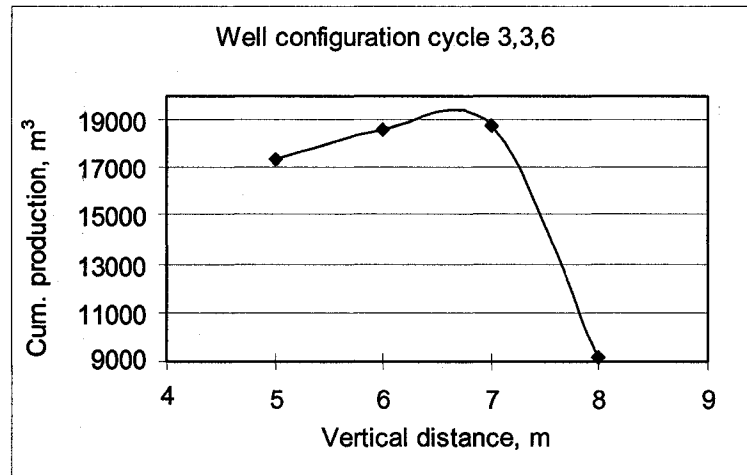


Figure 44. Sensitivity Analysis of Vertical Distance (3,3,6)

A vertical distance of seven meters gives the best cumulative oil rate. A distance of eight meters produces the worst result. When the injector and the producer are located too far from each other, the solvent is not effective enough to move the oil between the two wells. However, if the distance is too small, and the area between the two wells is not large enough, there is still some free solvent that has not been used. The difference between distances of five, six, and

seven meters distance is significant.

As for cycles 3,3,6,6,6, the same results were obtained: seven meters is the optimal vertical distance and 70 m is the optimal horizontal distance. Tables 24 and 25, and Figures 45 and 46 show the results.

Table 24. Sensitivity Analysis of Horizontal Distance (3,3,6,6,6)

Horizontal	50 m	60 m	70 m	80 m
Cumulative production m ³	31488	34306	35124	33880
Difference m ³	0	2818	3636	2392

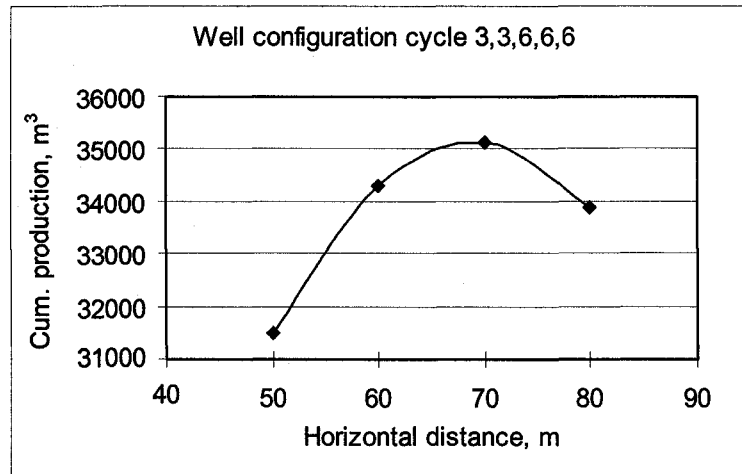


Figure 45. Sensitivity Analysis of Horizontal Distance (3,3,6,6,6)

The trend for cycles 3,3,6,6,6 is different from that of cycles 3,3,6. Instead of 80 m being the worst scenario for the horizontal distance, 50 m was the worst value for the longer cycles, which means that, when more solvent was injected, the interference between the two injectors increased. So, for longer cycles, a larger horizontal distance is preferred. There is a possibility that, for cycles even longer than the 3,3,6,6,6 cycles, the optimal horizontal distance could be changed to an even larger value.

Table 25. Sensitivity Analysis of Vertical Distance (3,3,6,6,6)

Vertical	5 m	6 m	7 m	8 m
Cumulative production, m ³	33869	35001	35124	29532
Difference, m ³	4337	5469	5592	0

With respect to the vertical distance, the longer cycles produced results similar to those of the shorter ones. These cycles all displayed a similar trend; however, the longer cycle had a smaller difference between the different options.

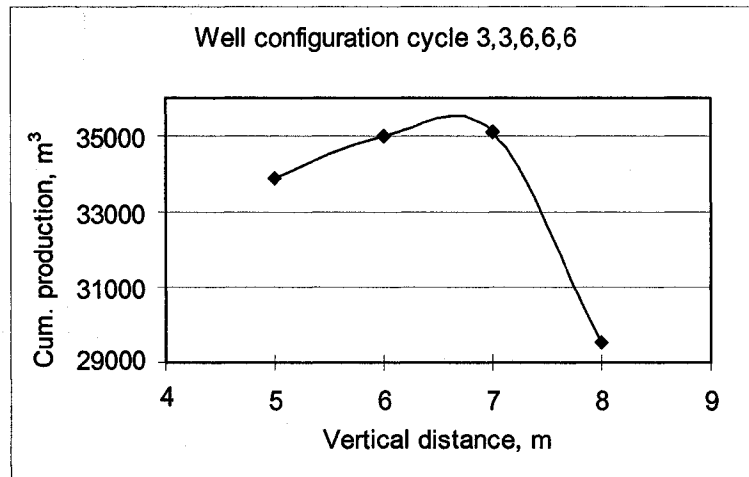


Figure 46. Sensitivity Analysis of Vertical Distance (3,3,6,6,6)

5.7 Recovery Factor

The recovery factor was calculated for the cycles 3,3,6 and 3,3,6,6,6 soaking cases, respectively, based on 5 m vertical distance between the injector and the producer and 70 m horizontal distance between the two well pairs. The results are as follows:

Cycle 3,3,6:

-OOIP: 345,015 m³

-Cumulative production: 17,332 m³

-Recovery factor: $17,332 / 345,015 = 5.02\%$

-Total solvent consumed: 1.57×10^6 kg

-NCSOR: 0.107

-Production life: $(3+4+12) \times 2 + (6+8+24) = 76$ months = 6.33 years

-Prorated yearly production: $17,332 / 6.33 = 2738.1$ m³/y

Cycles 3,3,6,6,6 soaking case:

-OOIP: 345,015 m³

-Cumulative production: 33,869 m³

-Recovery factor: $33,869 / 345,015 = 9.82\%$

-Total solvent consumed: 3.52×10^6 kg

-NCSOR: 0.109

-Production life: $(3+4+12) \times 2 + (6+8+24) \times 3 = 152$ months = 12.67 years

-Prorated yearly production: $33,869 / 12.67 = 2673$ m³/y

The recovery factor is pretty low. Cumulative production for cycles 3,3,6,6,6 is less than twice of that for cycles 3,3,6 although more than twice amount of solvent was consumed in cycle 3,3,6,6,6. The latter case shows a decline in peak production rate in the later stages of the production life, as shown in Figure 47.

The vertical distance between the injector and the producer will influence the overall NCSOR value significantly. For the cycles 3,3,6 case, the 5 m vertical distance yields a NCSOR value of 0.107; however, when this distance is increased to 7 m, it results in a much higher NCSOR value of 0.147. The reason for this is that the longer inter-well distance requires more time for the solvent to be transported from the injector to the producer.

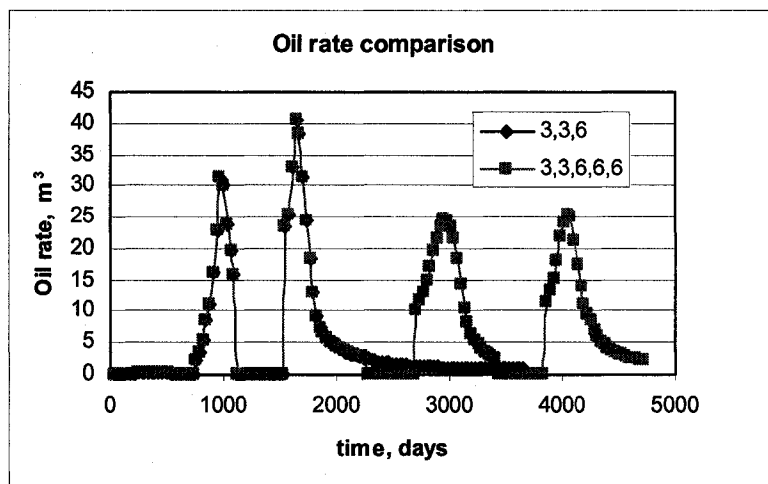


Figure 47. Oil rate comparison cycle 3,3,6 and 3,3,6,6,6

The 3D views of viscosity and oil saturation at the end of cycles 3,3,6 and cycles 3,3,6,6,6 are illustrated below in Figures 47 through 50.

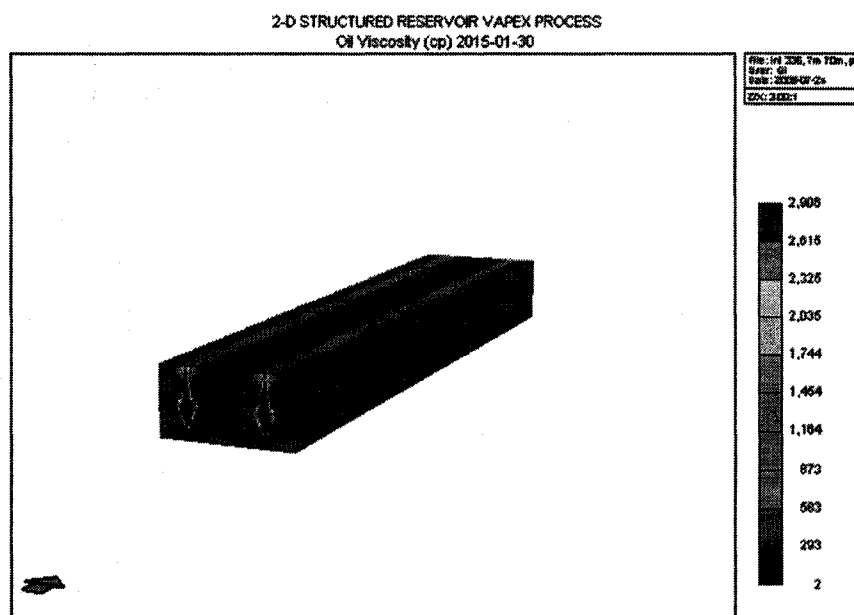


Figure 48. 3D view of oil viscosity at the end of cycles 3,3,6

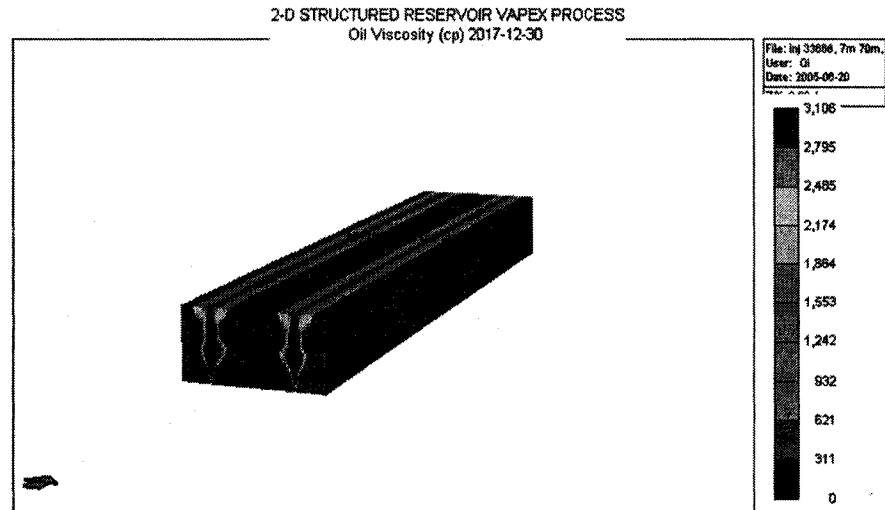


Figure 49. 3D view of oil viscosity at the end of cycles 3,3,6,6,6

The viscosity profiles of the long cycles (3,3,6,6,6) are compared with those of the short cycles (3,3,6) in Figures 48 and 49. The vapor chamber of the long cycles developed into a larger shape, but not twice as large as that of the short ones. Not much of the injected solvent in the short cycles reached the top of the reservoir; thus, the additional solvent in the longer cycles started to move to the upper level of the porous matrix and tried to sweep the untouched heavy oil from a previous cycle.

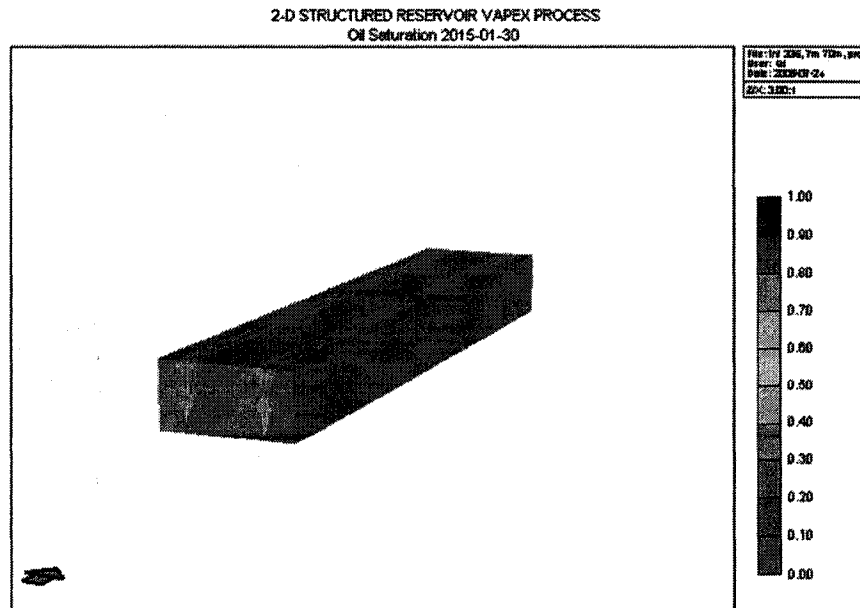


Figure 50. 3D view of oil saturation at the end of cycle 3,3,6

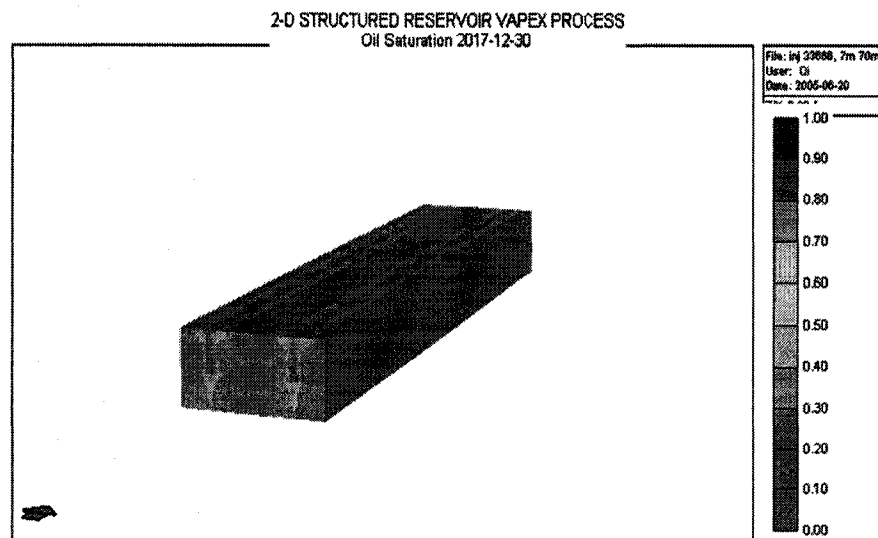


Figure 51. 3D view of oil saturation at the end of cycle 3,3,6,6,6

The 3D oil saturation images have similar expanding trends when compared with the viscosity images. As shown in Figures 49 and 51, the vapor chamber occupied around one-third of the total volume of the reservoir by the end of the cycles 3,3,6,6,6. At the center of the chamber, the oil saturation equals the residual oil saturation, and the viscosity has reached a very small value, which represents the solvent viscosity. However, at the edge of the chamber, the oil saturation and viscosity are much higher than those in the center. Similar trends can also be seen for the shorter cycles 3,3,6 (Figures 48 and 50).

As a result, more solvent is needed to sweep more oil from the reservoir matrix. The main mechanism in this cyclic solvent soaking process is gas push and dilution effect of the solvent on the heavy oil. Both the oil saturation and viscosity are smoothly distributed because of the homogeneous, ideally designed reservoir model.

The NCSOR of the long cycles was greater than that of the short cycles, indicating a less efficient recovery. This comparison of the short and long cycles was mainly for illustrative purposes, as optimization was not attempted.

CHAPTER 6

CONCLUSIONS AND SUGGESTIONS

The following conclusions and suggestions are summarized based on the simulation studies for this cyclic solvent injection process applied to mobile heavy oils.

- Some of the basic PVT data, such as CVD, CCE, DL, and Separator Test are necessary for tuning the EOS. For a solvent-based process, it is also important to conduct swelling tests of different multi-component solvents with the oil in order to adjust the binary interaction coefficients between individual hydrocarbons.
- The optimal solvent mixture could be obtained by examining the swelling test, which has been built into WinProp and further validated through thermodynamic simulations. The cumulative dissolved propane in the produced oil follows the same trend of cumulative production. The most effective solvent mixture could achieve the most cumulative production.
- The optimal solvent is case specific; it depends on the type of reservoir fluid, reservoir properties, and solvent injection rate.
- Ethane should not be an ingredient in the solvent mixture if the original reservoir fluid contains a considerable amount of methane. Ethane will reduce the saturation pressure significantly when it is injected into the reservoir fluid.
- Optimal soaking time can be found via the viscosity profile at the grid block, which is within the vapor chamber, GOR performance, and the cumulative production profile. However, if the injection time is not long enough, such as an initial injection period of three months, then the cumulative production is not obvious under different soaking period conditions.
- The most attractive NCSOR value was obtained for cycles 3,3,6; in another words, the short cycles at the beginning and a longer subsequent cycle will have good results. No

soaking has the worst NCSOR value. Thus, proper soaking is essential for the solvent-based heavy oil recovery method.

- The main mechanisms for this cyclic solvent injection process are gas push /pressure cycling and the dilution effect of the solvent on the heavy oil.
- Well configuration is another case dependent design parameter. In this study, the optimal vertical distance between the injector and the producer was found to be seven meters, and the optimal horizontal distance between the two well pairs 70 m.
- The vertical distance between the injector and the producer is more sensitive to the cumulative production than is the horizontal distance between the two well pairs.
- Two different cycles, one short (3,3,6) and one long (3,3,6,6,6) were compared in terms of recovery factor, NCSOR, and final viscosity and oil saturation profiles. Although twice as much solvent was consumed in the long cycles case, the recovery was less than double that of the short cycles case.
- The proposed cyclic solvent soaking process is a slow but effective method for producing mobile heavy oils. It still needs to be optimized.
- If appropriate data are available for the solvent-based process, economic analysis is recommended to evaluate the performance of different cycles and their corresponding no soaking cases. Properly designed soaking cases give the most attractive NSCOR results; however, the no soaking cases produce oil earlier.
- In the future, it is suggested that experiments be carried out to validate the simulation results and to better understand the main mechanisms involved in this solvent soaking process. The experimental results will be history matched by numerical simulation for the same solvent mixture and oil conditions used in this study. The key target parameter is the convective dispersion, which represents the combination of the two main mass transfer mechanisms, molecular diffusion and convective dispersion, in a solvent-based heavy oil recovery process.

REFERENCES

1. DAS, S.K., "An Efficient Process for the Recovery of Heavy Oil and Bitumen", SPE Journal 50941, September 1998.
2. JANISCH, A.: "Oil Sands and Heavy Oil: Can They Ease the Energy Shortage," First United Nations Inst. for Training and Research (UNITAR) Conference, Edmonton, Alberta (4-12 June 1979).
3. SINGHAL, A.K., LEGGITT, S.M., KASRAIE, M. and ITO, Y., "Screening of Reservoir for Exploitation by Application of Steam Assisted Gravity Drainage/Vapex Processes", SPE 37144, presented at the 1996 International Conference on Horizontal Well Technology held in Calgary, November 18-20, 1996.
4. WIGHTMAN, D., ROTTENFUSSER, B., KRAMERS, J., and HARRISON, R.: "Geology of Alberta Oil Sands Deposits," *AOSTRA Technical Handbook on Oil Sands, Bitumens and Heavy Oils*, 1989.
5. BROOK, G. and KANTZAS, A., "Evaluation of Non-thermal EOR Techniques for Heavy Oil Production", the Journal of Canadian Petroleum Technology 98-45, presented at 49th Annual Technical meeting of the Petroleum Society in Calgary, June 8-10, 1998.
6. BUTLER, R.M. and MOKRYS, I.J., "Recovery of Heavy Oil Using Vaporized Hydrocarbon Solvents Further Development of the VAPEX Process", the Journal of Canadian Petroleum Technology 93-06-06.
7. MOKRYS, I.J. and BUTLER, R.M., "In-Situ Upgrading of Heavy Oils and Bitumen by Propane De-asphalting: The VAPEX process", SPE 25452, presented at the Production Operations Symposium, Oklahoma City, Oklahoma, March 21-23, 1993.
8. DAS, S.K. and BUTLER, R.M., "Mechanisms of the Vapor Extraction for Heavy Oil and Bitumen", Journal of Petroleum Science and Engineering, Volume 21, 1998, page 43-59.

-
9. FRAUENFELD, T.V.J., KISSEL, G., and ZHOU, S.B., "PVT and Viscosity Measurements for Lloydminster - Alberfeldy and Cold Lake Blended Oil Systems ", SPE/Petroleum Society of CIM/CHOA 79018, presented at the 2002 SPE International Thermal Operations and Heavy Oil Symposium and International Horizontal Well Technology Conference, Calgary, Alberta, November 4-7, 2002.
 10. FISHER, D.B., SINGHAL, A.K., GOLDMAN, J., JACKSON, C. and RANDALL, L., "Insight from MRI and Micro-Model Studies of Transportation of Solvent into Heavy Oil during Vapex", SPE 79024, presented at the 2002 SPE International Thermal Operations and Heavy Oil Symposium and International Horizontal Well Technology Conference, Calgary, Alberta, November 4-7, 2002.
 11. DAUBA, C., QUETTIER, L., CHRISTENSEN, J., LE GOFF, C. and CORDELIER, P., "An Integrated Experimental and Numerical Approach to Assess the Performance of Solvent Injection into Heavy Oil", SPE 77459, presented at the SPE Annual Technical Conference and Exhibition, San Antonio, Texas, September 29–October 2, 2002.
 12. NGHIEM, L.X., KOHSE, B.F., FAROUQ ALI, S.M. and DOAN, Q., "Asphaltene Precipitation: Phase Behavior Modeling and Compositional Simulation", SPE 59432, presented at the 2000 SPE Asia Pacific Conference on Integrated Modeling for Asset Management, Yokohama, Japan, April 25-26, 2000.
 13. FRAUENFELD, T.J.W. and LILLICO D.A., "Solvent-assisted method for mobilizing viscous heavy oil ", United States Patent No. 5899274, September 20, 1996.
 14. BUTLER, R.M., MOKRYS, I, J and DAS, S.K., "The solvent Requirements for VAPEX Recovery", SPE 30293, presented at the International Heavy Oil Symposium held in Calgary, June 19-21 1995.
 15. FISHER, D.B., SINGHAL, A.K., DAS, S.K., GOLDMAN, J and JACKSON, C., "Use of Magnetic Resonance Imaging and Advanced Image Analysis as a Tool to Extract Mass Transfer Information from a 2D Physical Model of the VAPEX Process", SPE 59330, presented at the 2000 SPE/DOE Improved Oil Recovery Symposium held in

Tulsa, Oklahoma, April 3-5, 2002.

16. KARMAKER, K. and MAINI, B.B., "A Stochastic Approach to Extract Vapex related Dispersion coefficients from Magnetic Resonance Images," SPE 84198, presented at the SPE Annual Technical Conference and Exhibition, Denver, Colorado, Oct. 5 – 8, 2003.
17. YANG, C.D. and GU, Y.G., "A New Method for Measuring Solvent Diffusivity in Heavy Oil by Dynamic Pendant Drop Shape Analysis (DPDSA)", SPE 84202, presented at the SPE Annual Technical Conference and Exhibition, Denver, Colorado, Oct. 5 – 8, 2003.
18. BUTLER, R.M. and MOKRYS, I.J., "Solvent Analog Model of Steam-Assisted Gravity Drainage", AOSTRA Journal of Research 5, 17-32, 1989.
19. BOUSTANI, A. and MAINI, B.B., "The Role of Diffusion and Convective Dispersion in Vapor Extraction Process", Journal of Canadian Petroleum Technology, Vol. 40, No.4. (April 2001), pp. 68 - 77.
20. KARMAKER, K. and MAINI, B.B., "Experimental Investigation of Oil Drainage Rates in the VAPEX Process for Heavy Oil and Bitumen Reservoirs", SPE 84199, presented at the SPE Annual Technical Conference and Exhibition, Denver, Colorado, Oct. 5 – 8, 2003.
21. YAZDANI, A. and MAINI, B.B., "Effect of Drainage Height and Grain Size on the Convective Dispersion in the VAPEX Process: Experimental Study", SPE 89409, presented at the 2004 SPE/DOE Fourteenth Symposium On Improved Oil Recovery held in Tulsa Oklahoma, April 17-21, 2004.
22. QI, J. and BUTLER, R.M., "Selections of Well Configurations in VAPEX Process", SPE 37145, presented at the 1996 SPE International Conference on Horizontal Well Technology, Calgary, Alberta, November 18-20, 1996.
23. DAS, S.K. and BUTLER, R.M., "Counter Current Extraction of Heavy Oil and Bitumen", SPE 37094, presented at 1996 SPE International Conference on Horizontal

Well Technology, Calgary, Alberta, November 18-20, 1996.

24. KARMAKER, K. and MAINI, B.B., "Applicability of Vapor Extraction Process to Problematic Viscous Oil Reservoirs", SPE 84034, presented at the SPE Annual Technical Conference and Exhibition, Denver, Colorado, Oct. 5 – 8, 2003.
25. NGHIEM, L.X., KOHSE, B.F. and SAMMON, P.H., "Compositional Simulation of the VAPEX Process," *J. Can. Pet. Soc.*, Vol. 40, No. 8 (August 2001), pp. 54 – 61.
26. PERKINS, T.K. and JOHNSTON, O.C., "A Review of Diffusion and Dispersion in Porous Media", SPE Reprint Series, Miscible Displacement, pp 77-91, 1963.
27. HAYDUK, W., and MINHAS, B.S., "Correlations for Prediction of Molecular Diffusivities in Liquid", *Canadian Journal Chemical Engineering*. Vol. 60, pp. 295-299, April 1982.
28. HAYDUK, W., CASTANEDA, R., BROMFIELD, H. and PERRAS, R.R.. "Diffusivities of Propane in Normal Paraffin, Chlorobenzene, and Butanol Solvents", *AICHE Journal*, Vol. 19, No. 4, pp. 859-861, July 1973.
29. DAS, S.K. and BUTLER, R.M., "Diffusion coefficients of Propane and Butane in Peace River Bitumen", *Canadian Journal Chemical Engineering*, Vol. 74, No. 6, pp. 985-992, 1996.
30. NGHIEM, L.X., SAMMON, P.H., and KOHSE, B.F., "Modeling Asphaltene Precipitation and Dispersive Mixing in the Vapex Process," SPE 66361, presented at the SPE Reservoir Simulation Symposium, Houston, Texas, February 11-14, 2001.
31. NGHIEM, L.X., KOHSE, B.F., and FAROUQ ALI, S.M., "Asphaltene Precipitation: Phase Behavior Modeling and Compositional Simulation", SPE 59432, presented at the 2002 SPE Asia Pacific Conference on Integrated Modeling for Asset Management, Yokohama, Japan, April 25-26, 2000.
32. KOHSE, B.F. and NGHIEM, L.X., "Modeling Asphaltene Precipitation and Deposition in a Compositional Reservoir Simulator", SPE 89437, presented at the 2004 SPE/DOE Fourteenth Symposium on Improved Oil Recovery, Tulsa, Oklahoma, April 17-21,

-
- 2004.
33. COMPUTER MODELLING GROUP LTD., GEM manuals, Calgary, Alberta, October 2004.
 34. COMPUTER MODELLING GROUP LTD., STARS manuals, Calgary, Alberta, October 2004.
 35. COMPUTER MODELLING GROUP LTD., WinProp manuals, Calgary, Alberta, October 2004.
 36. PENG, D.Y. and ROBINSON, D.B., "A New Two-Constant Equation of State", *Ind. & Eng. Chem. Fund.* 1976 Vol. 15, No. 1 pp. 59-64.
 37. WHITSON, C. H., "Characterizing Hydrocarbon Plus Fractions", *Soc. Pet. Eng. J.* August 1983, 683-94.
 38. KATZ, D. L. and FIROOZABADI, A., "Prediction Phase Behavior of Condensate/Crude Oil System", *J. Pet. Tech.* Nov. 1978, 1649-55.
 39. COATS, K.H. and SMART, G.T., "Application of a Regression-Based EOS PVT Program to Laboratory Data," *SPE Reservoir Eng.* Vol. 1, No. 3, May 1986, pp. 277-299.
 40. DENNIS J.E., Jr., GAY, D.M., and WELSCH, R.E., "An Adaptive Nonlinear Least-Squares Algorithm," *ACM Trans. Math. Software*, Vol. 7, No. 3, September 1981, pp. 348-368.
 41. SOAVE, G, "Equilibrium Constants from a Modified Redlich-Kwong Equation of State", *Chem. Eng. Sic.*, 1972, Vol. 27. Pp.1197-1203.
 42. JESPERSEN, P.J. and FONTAINE, T.J.C, "The Tangleflags North Pilot: A Horizontal Well Steam-flood", Volume 32, No. 5, May 1993.
 43. DAVISON, R.J., "Electromagnetic Stimulation of Lloydminster Heavy Oil Reservoirs", Petroleum Society of CIM and CANMET, Paper No. 18, to be presented at the 4th Petroleum Conference of the South Saskatchewan Section, October, 1991.
 44. ESCOBAR, E., VALKO, P., LEE, W.J. and RODRIGUEZ, M.G., "Optimization

Methodology for Cyclic Steam Injection with Horizontal Wells” SPE/Petroleum Society of CIM 65525, presented at the 2000 SPE/Petroleum Society of CIM International Conference on Horizontal Well Technology, Calgary, Alberta, November 6-8, 2002.

45. HSU, H.H and BRUGMAN, R.J, “CO₂ Huff-Puff Simulation Using a Compositional Reservoir Simulator”, SPE 15503, presented at the 61st Annual Technical Conference and Exhibition of the Society of Petroleum Engineers held in New Orleans, LA October 5-8, 1986.

APPENDIX

APPENDIX 1. DATA FILE OF GEM

TITLE1 '2-D STRUCTURED RESERVOIR VAPEX PROCESS'

CASEID 'VAPEX-2D'

** =====input and output control=====**

*INUNIT *SI

REWIND 2

WRST TIME

WPRN WELL TIME

WPRN GRID TIME

WPRN ITER BRIEF

WSRF WELL TIME

WSRF GRID TIME

DIARY WELL-INFO

SUMMARY

DIM MAX_LAYERS 15

RANGECHECK ON

OUTPRN WELL BRIEF

OUTPRN GRID NONE

OUTPRN RES NONE

OUTSRF WELL XWEL 'C3' 'Hor. Producer' YWEL 'C3' 'Hor. Producer'

OUTSRF GRID DENG DENO KRG KRO KRW PRES SATP SG SO SW TSO

VISO X 'C1B' X 'C3' X 'C33+' Y 'C1B' Y 'C3' Z 'C1' Z 'C2' Z 'C3'

OUTSRF RES ALL

** =====Reservoir definition===== **

GRID CART 120 1 20

*DEPTH *TOP 1 1 1 450.

KDIR DOWN

DI CON 1.

DJ CON 600.

DK CON 1.

**\$ Property: NULL Blocks Max: 1 Min: 1

**\$ 0 = null block, 1 = active block

NULL CON 1

**\$ Property: Porosity Max: 0.33 Min: 0.33

POR CON 0.33

PERMI CON 2000.0

PERMJ EQUALSI

PERMK CON 1000

**\$ Property: Pinchout Array Max: 1 Min: 1

PINCHOUTARRAY CON 1

CPOR MATRIX 7.4E-06

**COMPOSITION *PRIMARY

** 2.3301035E-01 0.0000000E+00 0.0000000E+00 8.4906041E-05

** 3.3047420E-03 2.8450000E-01 1.5050000E-01 3.2860000E-01

**COMPOSITION *SECOND

** 0.0000000E+00 0.0000000E+00 0.0000000E+00 0.0000000E+00

** 0.0000000E+00 0.0000000E+00 0.0000000E+00 0.0000000E+00

**\$ Model and number of components

MODEL PR

NC 8 8

COMPNAME 'C1' 'C1B' 'C2' 'C3' 'C4toC6' 'C07-C23' 'C24-C32' 'C33+'
 HCFLAG 00000000
 VISCOR MODPEDERSEN
 VISCOEFF 1.0000E-04 2.51021E+00 8.853600E-03 1.8540401E+00 4.1390334E-01
 MW 16.043 16.043 30.07 44.097 83.2307 208.368 331.452 800
 AC 0.008 0.008 0.098 0.152 0.266855 0.55991 0.832716 1.42823
 PCRIT 45.4 45.4 48.2 41.9 32.7545 19.0238 13.7705 5.87161
 VCRIT 0.099 0.099 0.148 0.203 0.335719 0.752624 1.10512 2.07465
 TCRIT 190.6 190.6 305.4 369.8 499.119 727.844 846.383 1068.55
 PCHOR 77 77 108 150.3 244.766 566.111 817.498 1164.6
 SG 0.3 0.3 0.356 0.507 0.679188 0.845093 0.904373 1.03534
 TB -161.45 -161.45 -88.65 -42.05 60.0319 270.24 392.799 726.05
 OMEGA 0.457236 0.457236 0.457236 0.457236 0.457236 0.457236 0.457236 0.457236
 OMEGB 0.0777961 0.0777961 0.0777961 0.0777961 0.0777961 0.0777961 0.0777961 0.0777961
 0.0777961
 VSHIFT -0.153861 -0.153861 -0.102103 -0.0733009 -0.00969805 0.0969 0.07743 0.365319
 TRES 21

**\$ RESULTS PROP EOSTYPE Units: Dimensionless
 **\$ RESULTS PROP Minimum Value: 1 Maximum Value: 1

EOSTYPE CON 1.

=====Rock fluid properties=====

*ROCKFLUID

RPT 1 DRAINAGE

***** SWT*****

SWT

**\$	Sw	krw	krow	Pcow
	0.25	0	0.65	

0.3125	0.000277012	0.407325
0.34375	0.00114503	0.314264
0.40625	0.00684366	0.175133
0.4375	0.0129546	0.125457
0.46875	0.0222196	0.0867645
0.5	0.0354575	0.0574524
0.5625	0.0774272	0.0209905
0.59375	0.108086	0.0110889
0.625	0.146564	0.00507813
0.6875	0.251386	0.000448847
0.71875	0.320047	3.96729e-005
0.775	0.475857	0
0.8	0.56	0

**MODBUILDER *SMOOTH *ALLPL *DSLTI 0.05

SLT

**\$	SI	krq	krog
	0.45	0.8	0
	0.475	0.58997	0
	0.5	0.422625	0
	0.53125	0.26484	8.6632e-005
	0.5625	0.154408	0.000980129
	0.59375	0.081571	0.00405138
	0.609375	0.0564137	0.00694891
	0.625	0.0373552	0.0110889
	0.640625	0.0234088	0.0167464
	0.671875	0.00720992	0.0338024

0.6875	0.00330176	0.0458361
0.703125	0.00120631	0.0606562
0.75	0	0.125457
0.825	0	0.314264
0.9	0	0.65

*KROIL *STONE2 *SWSG

**\$ Property: Connate Water Saturation Max: 0.3 Min: 0.3

=====initial conditions=====

*INITIAL

VERTICAL DEPTH_AVE WATER_OIL EQUIL

*GASZONE *NOOIL

*NREGIONS 1

ZOIL 0.23301 0.0 0.00000 0.00008 0.00330 0.28450 0.15050 0.32860

REFPRES 4076

REFDEPTH 450.0001

DWOC 470.

SWOC 0.999999

**\$ RESULTS PROP ITYPE Units: Dimensionless

**\$ RESULTS PROP Minimum Value: 1 Maximum Value: 1

ITYPE CON 1.

*NUMERICAL

NORM PRESS 500

NORM SATUR 0.1

NORM GMOLAR 0.1

*NORTH 60

*ITERMAX 100

RUN

~~**=====well configuration=====**~~

DATE 2005 1 30

WELL 'Hor. Injector2'

INJECTOR 'Hor. Injector2'

INCOMP SOLVENT 0. 0.39 0. 0.61 0. 0. 0. 0.

OPERATE MAX STG 4500. CONT

**\$ rad geofac wfrac skin

GEOMETRY K 0.0762 0.37 1. 0.

PERF GEO 'Hor. Injector2'

**\$ UBA ff Status Connection

20 1 13 1. OPEN FLOW-FROM 'SURFACE'

OPEN 'Hor. Injector2'

WELL 'Hor Injector'

INJECTOR 'Hor Injector'

INCOMP SOLVENT 0. 0.39 0. 0.61 0. 0. 0. 0.

OPERATE MAX STG 4500. CONT

**\$ rad geofac wfrac skin

GEOMETRY K 0.0762 0.37 1. 0.

PERF GEO 'Hor Injector'

**\$ UBA ff Status Connection

100 1 13 1. OPEN FLOW-FROM 'SURFACE'

OPEN 'Hor Injector'

WELL 'Hor. Producer'

PRODUCER 'Hor. Producer'

OPERATE MIN BHP 4100. CONT

**\$ rad geofac wfrac skin

GEOMETRY K 0.0762 0.37 1. 0.

PERF GEO 'Hor. Producer'
**\$ UBA ff Status Connection
100 1 18 1. OPEN FLOW-TO 'SURFACE'
SHUTIN 'Hor. Producer'
WELL 'Hor producer2'
PRODUCER 'Hor producer2'
OPERATE MIN BHP 4100. CONT
**\$ rad geofac wfrac skin
GEOMETRY K 0.0762 0.37 1. 0.
PERF GEO 'Hor producer2'
**\$ UBA ff Status Connection
20 1 18 1. OPEN FLOW-TO 'SURFACE'
SHUTIN 'Hor producer2'
*AIMWELL WELLNN
*DTMAX 365.
DATE 2005 2 28
DATE 2005 3 30
DATE 2005 4 30
SHUTIN 'Hor Injector'
SHUTIN 'Hor. Injector2'
DATE 2005 5 30
DATE 2005 6 30
DATE 2005 7 30
DATE 2005 8 30
OPEN 'Hor producer2'
OPEN 'Hor. Producer'
INJECTOR 'Hor Injector'

INCOMP SOLVENT 0. 0.39 0. 0.61 0. 0. 0. 0.
OPERATE MAX BHP 4400. CONT
OPEN 'Hor Injector'
INJECTOR 'Hor. Injector2'
INCOMP SOLVENT 0. 0.39 0. 0.61 0. 0. 0. 0.
OPERATE MAX BHP 4400. CONT
OPEN 'Hor. Injector2'
DATE 2005 9 30
DATE 2005 10 30
DATE 2005 11 30
DATE 2005 12 30
DATE 2006 1 30
DATE 2006 2 28
DATE 2006 3 30
DATE 2006 4 30
DATE 2006 5 30
DATE 2006 6 30
SHUTIN 'Hor producer2'
SHUTIN 'Hor. Producer'
INJECTOR 'Hor Injector'
INCOMP SOLVENT 0. 0.39 0. 0.61 0. 0. 0. 0.
OPERATE MAX STG 4500. CONT
OPEN 'Hor Injector'
INJECTOR 'Hor. Injector2'
INCOMP SOLVENT 0. 0.39 0. 0.61 0. 0. 0. 0.
OPERATE MAX STG 4500. CONT
OPEN 'Hor. Injector2'

DATE 2006 7 30
DATE 2006 8 30
DATE 2006 9 30
SHUTIN 'Hor Injector'
SHUTIN 'Hor. Injector2'
DATE 2006 10 30
DATE 2006 11 30
DATE 2006 12 30
DATE 2007 1 30
OPEN 'Hor producer2'
OPEN 'Hor. Producer'
INJECTOR 'Hor Injector'
INCOMP SOLVENT 0. 0.39 0. 0.61 0. 0. 0. 0.
OPERATE MAX BHP 4400. CONT
OPEN 'Hor Injector'
INJECTOR 'Hor. Injector2'
INCOMP SOLVENT 0. 0.39 0. 0.61 0. 0. 0. 0.
OPERATE MAX BHP 4400. CONT
OPEN 'Hor. Injector2'
DATE 2007 2 28
DATE 2007 3 30
DATE 2007 4 30
DATE 2007 5 30
DATE 2007 6 30
DATE 2007 7 30
DATE 2007 8 30
DATE 2007 9 30

DATE 2007 10 30
DATE 2007 11 30
DATE 2007 12 30
DATE 2008 1 30
SHUTIN 'Hor producer2'
SHUTIN 'Hor. Producer'
INJECTOR 'Hor Injector'
INCOMP SOLVENT 0. 0.39 0. 0.61 0. 0. 0. 0.
OPERATE MAX STG 4500. CONT
OPEN 'Hor Injector'
INJECTOR 'Hor. Injector2'
INCOMP SOLVENT 0. 0.39 0. 0.61 0. 0. 0. 0.
OPERATE MAX STG 4500. CONT
OPEN 'Hor. Injector2'
DATE 2008 2 29
DATE 2008 3 30
DATE 2008 4 30
DATE 2008 5 30
DATE 2008 6 30
DATE 2008 7 30
SHUTIN 'Hor Injector'
SHUTIN 'Hor. Injector2'
DATE 2008 8 30
DATE 2008 9 30
DATE 2008 10 30
DATE 2008 11 30
DATE 2008 12 30

DATE 2009 1 30
DATE 2009 2 28
DATE 2009 3 30
OPEN 'Hor producer2'
OPEN 'Hor. Producer'
INJECTOR 'Hor Injector'
INCOMP SOLVENT 0. 0.39 0. 0.61 0. 0. 0. 0.
OPERATE MAX BHP 4400. CONT
OPEN 'Hor Injector'
INJECTOR 'Hor. Injector2'
INCOMP SOLVENT 0. 0.39 0. 0.61 0. 0. 0. 0.
OPERATE MAX BHP 4400. CONT
OPEN 'Hor. Injector2'
DATE 2009 4 30
DATE 2009 5 30
DATE 2009 6 30
DATE 2009 7 30
...
DATE 2015 1 30
STOP